J|A|C|S

ARTICLES

Synthesis and Photophysical Properties of Stilbeneoctasilsesquioxanes. Emission Behavior Coupled with Theoretical Modeling Studies Suggest a 3-D Excited State Involving the Silica Core

R. M. Laine,[*,†,▽] S. Sulaiman,[▽] C. Brick,[⊗] M. Roll,[▽] R. Tamaki,[†,⊥] M. Z. Asuncion,[▽] M. Neurock,[‡] J.-S. Filhol,[‡,#] C.-Y. Lee,[‡] J. Zhang,[⊗] T. Goodson III,[⊗] M. Ronchi,[§] M. Pizzotti,[§] S. C. Rand,[∥] and Y. Li[∥]

Departments of Materials Science and Engineering, Chemistry, and Macromolecular Science and Engineering, University of Michigan, Ann Arbor, Michigan 48109-2136, Department of Chemical Engineering, University of Virginia, Charlottesville, Virginia 22904-4741, Dipartimento di Chimica Inorganica Metallorganica e Analitica dell'Università di Milano "Lamberto Malatesta", Unità di Ricerca dell'INSTM, Via Venezian 21, 20133, Milano, Italy, and Department of Physics, University of Michigan, Ann Arbor, Michigan 48109-2122

Received October 14, 2009; E-mail: talsdad@umich.edu

Abstract: A set of stilbene-substituted octasilicates [p-RStil$_x$Ph$_{8-x}$SiO$_{1.5}$]$_8$ (R = H, Me, MeO, Cl, NMe$_2$ and x = 5.3−8) and [o-MeStilSiO$_{1.5}$]$_8$ were prepared. Model compounds were also prepared including the corner and half cages: [p-MeStilSi(OEt)$_3$], [p-Me$_2$NStilSi(OSiMe$_3$)$_3$], and [p-Me$_2$NStilSi(O)(OSiMe)]$_4$. These compounds were characterized by MALDI-TOF, TGA, FTIR, and ^{1}H NMR techniques. Their photophysical properties were characterized by UV−vis, two-photon absorption, and cathodoluminescence spectroscopy (on solid powders), including studies on the effects of solvent polarity and changes in concentration. These molecules are typically soluble, easily purified, and robust, showing $T_{d(5\%)}$ > 400 °C in air. The full and partial cages all show UV−vis absorption spectra (in THF) identical to the spectrum of *trans*-stilbene, except for [o-MeStilSiO$_{1.5}$]$_8$, which exhibits an absorption spectrum blue-shifted from *trans*-stilbene. However, the partial cages show emissions that are red-shifted by ∼20 nm, as found for stilbene−siloxane macrocycles, suggesting some interaction of the silicon center(s) with the stilbene π^* orbital in both the corner and half cages. In contrast, the emission spectra of the full cages show red-shifts of 60−100 nm. These large red-shifts are supported by density functional theoretical calculations and proposed to result from interactions of the stilbene π^* orbitals with a LUMO centered within the cage that has 4A_1 symmetry and involves contributions from all Si and oxygen atoms and the organic substituents. Given that this LUMO has 3-D symmetry, it appears that all of the stilbene units interact in the excited state, consistent with theoretical results, which show an increased red-shift with an increase in the functionalization of a single corner to functionalization of all eight corners with stilbene. In the case of the Me$_2$N- derivatives, this interaction is primarily a charge-transfer interaction, as witnessed by the influence of solvent polarity on the emission behavior. More importantly, the two-photon absorption behavior is 2−3 times greater on a per p-Me$_2$Nstilbene basis for the full cage than for the corner or half cages. Similar observations were made for p-NH$_2$stilbenevinyl$_8$OS cages, where the greater conjugation lengths led to even greater red-shifts (120 nm) and two-photon absorption cross sections. Cathodoluminescence studies done on [p-MeStilSiO$_{1.5}$]$_8$ or [p-MeStilOS]$_8$ powders exhibit essentially the same emissions as seen in solution at high dilution. Given that only the emissions are greatly red-shifted in these molecules, whereas the ground-state UV−vis absorptions are not changed from *trans*-stilbene, except for the ortho derivative, which is blue-shifted 10 nm. It appears that the interactions are only in the excited state. Theoretical results show that the HOMO and LUMO states are always the π and π^* states on the stilbene, which show very weak shifts with increasing degrees of functionalization, consistent with the small changes in the UV−vis spectra. The band gap between the lowest unoccupied 4a1 symmetry core state localized inside the silsesquioxane cage and the highest occupied state (π state on stilbene), however, is markedly decreased as the number of stilbene functional groups is increased. This is consistent with the significant red-shifts in the emission spectra. The results suggest that the emission occurs from the 4a1 state localized on the cage. Moreover, for the compounds [p-RStil$_{6-7}$Ph$_{2-1}$OS]$_8$, the emissions are blue-shifted compared to those of the fully substituted compounds, suggesting the molecular symmetry is reduced (from cubic), thereby reducing the potential for 3-D delocalization and raising the energy of the LUMO. The implications are that these octafunctional molecules exhibit some form of 3-D interaction in the excited state that might permit their use as molecular transistors as well as for energy collection and dispersion as molecular antennas, for example, and for nonlinear optical applications.

1. Introduction

Polyhedral silsesquioxanes (SQs) and materials based on them have witnessed a recent explosion in interest, as evidenced by the fact that there are now 11 reviews on the subject, with Figure 8 from ref 10 illustrating the fact that recently up to 200 publications and patents appear each year.[1−11] Part of this comes from their ease of synthesis and purification, their robust nature compared to most traditional organic molecules, and the facility with which their functionalities can be manipulated to suit particular applications.[12−39] Additional interest comes from the fact that it is possible to introduce 8, 16, and recently 24 functional groups to the core molecular structures, providing potential access to novel star, dendrimer, and hyperbranched compounds.[26−28,40] Most recently, SQ derivatives have found their way into electronic materials as low k dielectrics and in photonic materials as platforms for multiple components in organic light-emitting device (OLED) structures.[11,41−50]

In the course of these studies, there have also been more than 10 theoretical studies that attempted to assess the properties of SQ materials.[51−63] A subset of these studies were directed toward understanding their electronic structures and, in particular, their interactions with encapsulated ions. Based on these studies, the general consensus is that the highest occupied molecular orbital (HOMO) involves 2p lone-pair states of A_{2g} symmetry on the oxygen atoms. Likewise, it appears that the lowest unoccupied molecular orbital (LUMO) has $4A_1$ symmetry and involves contributions from all Si and oxygen atoms and the organic

† Department of Materials Science and Engineering, University of Michigan.
⊗ Department of Chemistry, University of Michigan.
▽ Department of Macromolecular Science and Engineering, University of Michigan.
‖ Department of Physics, University of Michigan.
‡ University of Virginia.
§ Università di Milano "Lamberto Malatesta".
⊥ Present address: Quallion Inc., Sylmar, CA 94303.
Present address: Chimie Théorique, Méthodologie, Modélisation, Institut Charles Gerhardt, Université Montpellier II, Montpellier, France.

(1) Voronkov, M. G.; Lavrent'yev, V. I. *Top. Curr. Chem.* **1982**, *102*, 199.
(2) Baney, R. H.; Itoh, M.; Sakakibara, A.; Suzuki, T. *Chem. Rev.* **1995**, *95*, 1409.
(3) Lichtenhan, J. In *Polymeric Materials Encyclopedia*; Salmone, J. C., Ed.; CRC Press: New York, 1996; Vol. 10, p 7768.
(4) Provatas, A.; Matisons, J. G. *Trends Polym. Sci.* **1997**, *5*, 327.
(5) Duchateau, R. *Chem. Rev.* **2002**, *102*, 3525.
(6) Abe, Y.; Gunji, T. *Prog. Polym. Sci.* **2004**, *29*, 149.
(7) Phillips, S. H.; Haddad, T. S.; Tomczak, S. J. *Curr. Opin. Solid State Mater. Sci.* **2004**, *8*, 21.
(8) Hanssen, R. W. J. M.; van Santen, R. A.; Abenhuis, H. C. L. *Eur. J. Inorg. Chem.* **2004**, 675.
(9) Laine, R. M. *J. Mater. Chem.* **2005**, *15*, 3725.
(10) Lickiss, P. D.; Rataboul, F. *Adv. Organomet. Chem.* **2008**, *57*, 1.
(11) Chan, K. L.; Sonar, P.; Sellinger, A. *J. Mater. Chem.* **2009**, *19*, 9013.
(12) (a) Hoebbel, D.; Pitsch, I.; Heidmann, D. *Eurogel '91*; Elsevier Sci. Publ.: Amsterdam, 1992; p 467. (b) Hoebbel, D.; Endres, K.; Reinert, T.; Pitsch, I. *J. Noncryst. Sol.* **1994**, *176*, 179.
(13) (a) Weidner, R.; Zeller, N.; Deubzer, B.; Frey, V. U.S. Patent 5,047,492, Sept 1991. (b) Dathe, S.; Popowski, E.; Sonnek, G.; Feiher, T.; Jancke, H.; Schelm, U. European Patent 0,348,705 A1, 1989. (c) Freyer, C.; Wolferseder, J.; Peetz, U. European Patent 0,624,691 A1 1993.
(14) Harrison, P. G.; Hall, C. *Main Group Metal Chem.* **1997**, *20*, 515.
(15) (a) Waddon, A. J.; Coughlin, E. B. *Chem. Mater.* **2003**, *15*, 4555. (b) Cardoen, G.; Coughlin, E. B. *Macromolecules* **2004**, *37*, 5123.
(16) (a) Fu, B. X.; Hsiao, B. S.; White, H.; Rafailovich, M.; Mather, P.; Joen, H. G.; Phillips, S.; Lichtenhan, J.; Schwab, J. *Polym. Int.* **2000**, *49*, 437. (b) Fu, B. X.; Zhang, W.; Hsiao, B. S.; Rafailovich, M.; Sokolov, J.; Johansson, G.; Sauer, B. B.; Phillips, S.; Blanski, R. *High Performance Polym.* **2001**, *12*, 565.
(17) Lin, H.-C.; Kuo, S.-W.; Huang, C.-F.; Chang, F.-C. *Macromol. Rapid Commun.* **2006**, *27*, 537.
(18) (a) Baker, E. S.; Gidden, J.; Anderson, S. E.; Haddad, T. S.; Bowers, M. T. *Nano Lett.* **2004**, *4*, 779. (b) Fu, B. X.; Lee, A.; Haddad, T. S. *Macromolecules* **2004**, *37*, 5211. (c) Kopesky, E. T.; Haddad, T. S.; Cohen, R. E.; McKinley, G. H. *Macromolecules* **2004**, *37*, 8992.
(19) (a) Tuteja, A.; Choi, W.; Ma, M.; Mabry, J. M.; Mazella, S. A.; Rutledge, G. C.; McKinley, G. H.; Cohen, R. E. *Science* **2007**, *318*, 1618. (b) Mabry, J. M.; Vij, A.; Iacono, S. T.; Viers, B. D. *Angew. Chem., Int. Ed.* **2008**, *47*, 4137.
(20) (a) Kim, G.-M.; Qin, H.; Fang, X.; Sun, F. C.; Mather, P. T. *J. Polym. Sci. B: Polym. Phys.* **2003**, *41*, 3299. (b) Kim, B. S.; Mather, P. T. *Macromolecules* **2002**, *35*, 8378.
(21) (a) Choi, J.; Harcup, J.; Yee, A. F.; Zhu, Q.; Laine, R. M. *J. Am. Chem. Soc.* **2001**, *123*, 11420. (b) Choi, J.; Yee, A. F.; Laine, R. M. *Macromolecules* **2003**, *15*, 5666.
(22) (a) Tamaki, R.; Tanaka, Y.; Asuncion, M. Z.; Choi, J.; Laine, R. M. *J. Am. Chem. Soc.* **2001**, *123*, 12416. (b) Tamaki, R.; Choi, J.; Laine, R. M. *Chem. Mater.* **2003**, *15*, 793. (c) Choi, J.; Tamaki, R.; Kim, S. G.; Laine, R. M. *Chem. Mater.* **2003**, *15*, 3365.
(23) Neumann, D.; Fisher, M.; Tran, L.; Matisons, J. G. *J. Am. Chem. Soc.* **2002**, *124*, 13998.
(24) Maitra, P.; Wunder, S. L. *Chem. Mater.* **2002**, *14*, 4494.
(25) Mehl, G. H.; Goodby, J. W. *Angew. Chem.* **1996**, *35*, 2641.
(26) Feher, F. J.; Soulivong, D.; Eklund, A. G.; Wyndham, K. D. *Chem. Commun.* **1997**, 1185.
(27) (a) Dvornic, P. R.; Hartmann-Thompson, C.; Keinath, S. E.; Hill, E. J. *Macromolecules* **2004**, *37*, 7818. (b) Hong, B.; Thoms, T. P. S.; Murfee, H. J.; Lebrun, H. J. *Inorg. Chem.* **1997**, *36*, 6146. (c) Feher, F. J.; Wyndham, K. D. *Chem. Commun.* **1998**, 323.
(28) Brick, C. M.; Ouchi, Y.; Chujo, Y.; Laine, R. M. *Macromolecules* **2005**, *38*, 4661.
(29) (a) Adachi, K.; Tamaki, R.; Chujo, Y. *Bull. Chem. Soc. Jpn.* **2004**, *77*, 2115. (b) Kim, K.-M.; Chujo, Y. *J. Polym. Sci. A. Polym. Chem.* **2003**, *41*, 1309.
(30) Liu, H.; Kondo, S.-I.; Takeda, N.; Unno, M. *J. Am. Chem. Soc.* **2008**, *130*, 10074.
(31) Takahashi, K.; Sulaiman, S.; Katzenstein, J. M.; Snoblen, S.; Laine, R. M. *Aust. J. Chem.* **2006**, *59*, 564.
(32) Zhang, Z. L.; Horsch, M. A.; Lamm, M. H.; Glotzer, S. C. *Nano Lett.* **2003**, *3*, 1341.
(33) (a) Marciniec, B.; Pietraszuk, C. *Curr. Org. Chem.* **2003**, *7*, 691. (b) Kujawa-Welten, M.; Pietraszuk, C.; Marciniec, B. *Organometallics* **2002**, *21*, 840. (c) Itami, Y.; Marciniec, B.; Kubicki, M. *Chem.—Eur. J.* **2004**, *10*, 1239.
(34) (a) Sulaiman, S.; Brick, C. M.; De Sana, C. M.; Katzenstein, J. M.; Laine, R. M.; Basheer, R. A. *Macromolecules* **2006**, *39*, 5167. (b) Asuncion, M. Z.; Laine, R. M. *Macromolecules* **2007**, *40*, 555.
(35) Brick, C.; Chan, E. R.; Glotzer, S. C.; Martin, D. C.; Laine, R. M. *Adv. Mater.* **2007**, *19*, 82.
(36) (a) Takamura, N.; Viculis, L.; Laine, R. M. *Polym. Int.* **2007**, *56*, 1378. (b) Laine, R. M.; Roll, M.; Asuncion, M.; Sulaiman, S.; Popova, V.; Bartz, D.; Krug, D. J.; Mutin, P. H. *J. Sol-Gel Sci. Technol.* **2008**, *46*, 335.
(37) (a) Lichtenhan, J. D.; Vu, H. Q.; Carter, J. A.; Gilman, J. W.; Feher, F. J. *Macromolecules* **1993**, *26*, 2141. (b) Gilman, J. W.; Schlitzer, D. S.; Lichtenhan, J. D. *J. Appl. Polym. Sci.* **1996**, *60*, 591. (c) Gonzalez, R. I.; Phillips, S. H.; Hoflund, G. B. *J. Spacecraft Rockets* **2000**, *37*, 463.
(38) McCusker, C.; Carroll, J. B.; Rotello, V. M. *Chem. Commun.* **2005**, 996.
(39) (a) Zhang, Y.; Lee, S. H.; Liang, K.; Toghiani, H.; Pittman, C. U. *Polymer* **2006**, *47*, 2984. (b) Patel, R. R.; Mohanraj, R.; Pittman, C. U. *J. Polym. Sci. Part B—Polym. Phys.* **2006**, *44*, 234. (c) Liang, K.; Li, G. Z.; Toghiani, H.; Koo, J. H.; Pittman, C. U. *Chem. Mater.* **2006**, *18*, 301.
(40) (a) Roll, M.; Laine, R. M., manuscript in preparation. (b) Roll, M. Supermolecular Construction Using Octaphenylsilsesquioxane Derivatives. Ph.D. dissertation, University of Michigan, October 2009.
(41) Kim, H.-J.; Lee, J.-K.; Kim, J.-B.; Park, E. S.; Park, S.-J.; Yoo, D. Y.; Yoon, D. Y. *J. Am. Chem. Soc.* **2001**, *123*, 12121.
(42) Ro, H. W.; Char, K.; Jeon, E.-C.; Kim, H.-J.; Kwon, D.; Lee, H.-J.; Le, J.-K.; Rhee, H.-W.; Soles, C. L.; Yoon, D. Y. *Adv. Mater.* **2007**, *19*, 705.
(43) Imae, I.; Kawakami, Y. *J. Mater. Chem.* **2005**, *15*, 4581.
(44) Cho, H.-J.; Hwang, D.-H.; Lee, J.-I.; Jung, Y.-K.; Park, J.-H.; Lee, J.; Lee, S.-K.; Shim, H.-K. *Chem. Mater.* **2006**, *18*, 3780.
(45) (a) Froehlich, J. D.; Young, R.; Nakamura, T.; Ohmori, Y.; Li, S.; Mochizuki, A.; Lauters, M. *Chem. Mater.* **2007**, *19*, 4991. (b) Singh, B. B. M.; Chae, H. S.; Froehlich, J. D.; Kondou, T.; Li, S.; Mochizuki, A.; Jabbour, G. E. *Soft Matter* **2009**, *5*, 3002.

substituents, is spherical, and resides in the core center. This LUMO is considered to be highly electrophilic and is the reason that it is possible to encapsulate F⁻ ions in a wide variety of these compounds, providing that the organic substituents are at least mildly electron withdrawing.[58,59,64,65] The formation of cage-encapsulated F⁻ was calculated to be favored by as much as −60 to −80 kcal/mol.[59,65] In contrast, hydrogen atoms can be trapped within the cage as kinetic products, but calculations indicate that energetics are more favorable with the H atom outside the cage, in keeping with the idea that the center is highly electrophilic.[61,66]

A further general observation of these modeling studies is that the LUMO−HOMO gap for the simplest cages falls between 6 and 7 eV[52,54,55,57] for cages with H or alkyl groups at the corners. This contrasts with measured values of 4.0−4.4 eV for these same compounds.[53] The addition of aryl groups to the corners introduces π and π^* interactions that can be expected to lead to electronic transitions localized solely on the organics because of their smaller LUMO−HOMO gaps. On this basis, one might expect aromatic moieties to behave much the same as they do without being bound to a SQ cage. Indeed, this is found in most instances, as noted in studies directed toward using the cage to support moieties of use for photonic applications such as OLEDs.[11,43–50] However, in these instances there is no direct conjugation with the cage Si atoms except where vinyl pyrene moieties were introduced.[46b]

In contrast, we recently reported the synthesis of a set of silsesquioxane stars wherein a set of para H-, Me-, MeO-, and NH₂-substituted vinylstilbenes were linked directly to the cage through a vinyl group.[67] This set of compounds exhibited photophysical behaviors wherein the MeO- and NH₂- compounds showed very large red-shifts in their emissions relative to the parent vinylstilbene of 80−100 nm as the solvent was changed from hexane to acetonitrile. These shifts are similar to those expected if an electron-withdrawing cyano or nitro group were bound to the vinyl group rather than the cage.

The most logical explanation for this behavior is the existence of a charge-transfer (CT) transition in the excited state wherein electron donation occurs from the NH₂- (MeO-) group into the LUMO within the cage. Support for CT behavior comes from the observation of a very high two-photon cross section for this molecule [δ(GM) = 810 at 720 nm]. Given the symmetry of the LUMO calculated via multiple groups, it seems possible to argue that all eight moieties on the cage are involved and furthermore interact in the excited state. One possible implication is that we observe 3-D electronic interactions in the excited state.

In an effort to further our understanding of this behavior, we herewith present additional evidence favoring these conclusions from studies of stilbene systems connected to the silsesquioxane cage via phenyl rather than vinyl groups.

2. Experimental Section

2.1. Materials. Tetrahydrofuran (THF) and 1,4-dioxane were purchased from Fisher Scientific and distilled under nitrogen from Na/benzophenone ketyl prior to use. Methylene chloride (CH_2Cl_2) and acetonitrile (CH_3CN) were also purchased from Fisher Scientific and distilled from CaH_2 under nitrogen prior to use. Octaphenyl-octasilsesquioxane, $[PhSiO_{1.5}]_8$ or OPS, was synthesized according to procedures developed by Kim et al.[68] or received as a gift from Mayaterials Inc. All other chemicals were purchased from Aldrich or Fisher and used as received.

2.2. Synthesis Procedures. Synthesis of (BrPh)₅₋₆(Ph)₃₋₂OS. This compound was synthesized using literature methods which use iron-based catalysts and provide materials that are mostly para-substituted.[28] Alternately, a more recently developed synthesis was used that provides more uniform substitution but also provides materials that are mostly ortho-substituted, as described in the following.[40]

To a dry 100 mL Schlenk flask under N₂ was added 10 mL of CH_2Cl_2 via addition funnel followed by Br₂ (6.5 mL, 127 mmol, 1.64 mol/phenyl), and then 15 mL of CH_2Cl_2 was added to wash the funnel. The flask was cooled to ∼−50 °C in an ethylene glycol/ethanol/dry ice bath for ∼30 min. At that point OPS (10.0 g, 9.7 mmol, 77 mmol phenyl) was added slowly, ∼1 g/min, to the dark red solution. Following the addition, the N₂ flow was stopped, a vent to a bubbler containing aqueous base was added, and the solution was allowed to warm to ambient. The solution was stirred for 2 d at room temperature. Thereafter, ∼15 mL of H₂O was added, and the flask was placed in an ice bath. A saturated solution of sodium metabisulfite was added slowly, *with vigorous stirring*, until the bromine color disappeared (∼10−20 mL). The mixture was transferred to a separatory funnel, and the organic layer was extracted and washed sequentially with three 50 mL portions of water, ∼0.1 M sodium bicarbonate, and finally brine. The organic layer was filtered off and then dried with sodium sulfate to give a

(46) (a) Sellinger, A.; Tamaki, R.; Laine, R. M.; Ueno, K.; Tanabe, H.; Williams, E.; Jabbour, G. E. *Chem. Commun.* **2005**, 3700. (b) Lo, M. Y.; Zhen, C.; Lauters, M.; Jabbour, G. E.; Sellinger, A. *J. Am. Chem. Soc.* **2007**, *129*, 5808.

(47) Xaio, S.; Nguyen, M.; Gong, X.; Cao, Y.; Wu, H.; Moses, D.; Heeger, A. J. *Adv. Funct. Mater.* **2003**, *13*, 25.

(48) Chou, C.-H.; Hsu, S.-L.; Dinakaran, K.; Chiu, M.-Y.; Wei, K.-H. *Macromolecules* **2005**, *38*, 745.

(49) Lin, W.-J.; Chen, W.-C.; Wu, W.-C.; Niu, Y.-H.; Jen, A. K.-Y. *Macromolecules* **2004**, *37*, 2335.

(50) Miyake, J.; Chujo, Y. *Macromol. Rapid Commun.* **2008**, *29*, 86.

(51) (a) Calzaferri, G.; Hoffman, R. *J. Chem. Soc., Dalton Trans.* **1991**, 917. (b) Calzaferri, G. In *Tailor-made Silicon-Oxygen Compounds, from molecules to materials*; Corriu, R., Jutzi, P., Eds.; Publ. Friedr. Vieweg & Sohn mbH: Braunschweig/Weisbaden, Germany, 1996; pp 149−169.

(52) Schneider, K. S.; Zhang, Z.; Banaszak-Holl, M.; Orr, B. G.; Pernisz, U. C. *Phys. Rev. Lett.* **2000**, *85*, 602.

(53) Chen, Y.; Schneider, K. S.; Banaszak Holl, M.; Orr, B. G. *Phys. Rev. B* **2004**, *70*, 085402.

(54) (a) Ossadnik, C.; Veprek, S.; Marsmann, H. C.; Rikowski, E. *Monatsch. Chem.* **1999**, *130*, 55. (b) Azinovic, D.; Cai, J.; Eggs, C.; Konig, H.; Marsmann, H. C.; Veprek, S. *J. Lumin.* **2002**, *97*, 40.

(55) Xiang, K.-H.; Pandy, R.; Pernisz, U. C.; Freeman, C. *J. Phys. Chem. B* **1998**, *102*, 8704.

(56) Cheng, W.-D.; Xiang, K.-H.; Pandey, R.; Pernisz, U. C. *J. Phys. Chem. B* **2000**, *104*, 6737.

(57) Lin, T.; He, C.; Xaio, Y. *J. Phys. Chem. B* **2003**, *107*, 13788.

(58) Anderson, S. E.; Bodzin, D. J.; Haddad, T. S.; Boatz, J. A.; Mabry, J. M.; Mitchell, C.; Bowers, M. T. *Chem. Mater.* **2008**, *20*, 4299.

(59) Park, S. S.; Xiao, C.; Hagelberg, F.; Hossain, D.; Pittman, C. U., Jr.; Saebo, S. *J. Phys. Chem. A* **2004**, *108*, 11260.

(60) (a) Li, H.-C.; Lee, C.-Y.; McCabe, C.; Striolo, A.; Neurock, M. *J. Phys. Chem. A* **2007**, *111*, 3577. (b) Striolo, A.; McCabe, C.; Cummings, P. T. *J. Phys. Chem. B* **2005**, *109*, 14300.

(61) Mattori, M.; Mogi, K.; Sakai, Y.; Isobe, T. *J. Phys. Chem. A* **2000**, *104*, 10868, and references therein.

(62) Ionescu, T. C.; Qi, F.; McCabe, C.; Striolo, A.; Kieffer, J.; Cummings, P. T. *J. Phys. Chem. B* **2006**, *110*, 2502.

(63) Cummings, P.; Glotzer, S.; Kieffer, J.; McCabe, C.; Neurock, M. *J. Comp. Theor. Nanosci.* **2004**, *1*, 265.

(64) Bassindale, A. R.; Pourny, M.; Taylor, P. G.; Hursthouse, M. B.; Light, M. E. *Angew. Chem., Int. Ed.* **2003**, *42*, 3488.

(65) Bassindale, A. R.; Parker, D. J.; Pourny, M.; Taylor, P. G.; Horton, P. N.; Hursthouse, M. B. *Organometallics* **2004**, *23*, 4400.

(66) Pach, M.; Stösser, R. *J. Phys. Chem. A* **1997**, *101*, 8360.

(67) Sulaiman, S.; Brick, C.; Roll, M.; Bhaskar, A.; Goodson, T.; Zhang, J.; Laine, R. M. *Chem. Mater.* **2008**, *20*, 5563.

(68) Kim, S.-G.; Sulaiman, S.; Fargier, D.; Laine, R. M. In *Materials Syntheses. A Practical Guide*; Schubert, U., Hüsing, N., Laine, R. M., Eds.; Springer-Verlag: Wein, 2008; pp 179−182.

clear, colorless liquid. Solvent was removed by rotary evaporation. The resulting solid was redissolved in THF and then precipitated into ~1 L of stirred, cold methanol. After filtration, addition of a few percent by volume of water to the filtrate yielded ~10% additional material. The precipitate was dried under vacuum to yield 13.7 g (8.2 mmol) of white powder (85% yield).

Synthesis of I$_8$OPS. This material was synthesized using the published procedure.[69]

Synthesis of [StilbeneSiO$_{1.5}$]$_8$. This material was synthesized using the published procedure.[69]

Synthesis of [MeStilbeneSiO$_{1.5}$]$_{6.8}$[PhSiO$_{1.5}$]$_{1.2}$ from (*p*-I-Ph)$_{6.8}$-(Ph)$_{1.2}$OS. I$_{6.8}$OPS was first prepared using the published preparation,[69] but with only 90% ICl. To a dry 25 mL Schlenk flask under N$_2$ were added 0.50 g (1.80 mmol -I) of I$_{6.8}$OPS, 18 mg (0.02 mmol, 1 mol %) of Pd$_2$(dba)$_3$, 19 mg (0.04 mmol, 2 mol %) of Pd[P(*t*-Bu)$_3$]$_2$, and 1.0 g of copper metal. 1,4-Dioxane (10 mL) was then added via syringe, followed by 0.78 mL (5.88 mmol) of 4-methylstyrene and 0.42 mL (1.96 mmol) of NCy$_2$Me. The mixture was stirred at room temperature for 48 h and then quenched by filtering through Celite. The filtrate was precipitated into 200 mL of methanol and filtered, and the solid was redissolved in 10 mL of THF. This solution was then filtered again through Celite to remove any remaining Pd particles and reprecipitated into 200 mL of methanol, and the solids were collected by suction filtration, providing a fine white powder in 86% yield.

Synthesis of [MeStilbeneSiO$_{1.5}$]$_8$ from I$_8$OPS. To a dry 25 mL Schlenk flask under N$_2$ were added 0.50 g (1.96 mmol -I) of I$_8$OPS, 18 mg (0.02 mmol, 1 mol %) of Pd$_2$(dba)$_3$, 19 mg (0.04 mmol, 2 mol %) of Pd[P(*t*-Bu)$_3$]$_2$ and 1.0 g of copper metal. 1,4-Dioxane (10 mL) was then added via syringe, followed by 0.78 mL (5.88 mmol) of 4-methylstyrene and 0.42 mL (1.96 mmol) of NCy$_2$Me. The mixture was stirred at room temperature for 48 h and then quenched by filtering through Celite. The filtrate was precipitated into 200 mL of methanol and filtered, and the solid was redissolved in 10 mL of THF. This solution was then filtered again through Celite to remove any remaining Pd particles and reprecipitated into 200 mL of methanol, and the solids were collected by suction filtration, providing a 62% yield of crude material. The obtained white powder was purified by column chromatography (hexane:THF 80:20) to give a 21% yield of purified material.

Synthesis of *o*-MeStilbene$_8$OS from *o*-BrPh$_8$OS. To a dry 10 mL Schlenk flask under N$_2$ were added 0.50 g (2.40 mmol -Br) of *o*-BrPh$_8$OS,[40] 21 mg (0.023 mmol, 1 mol %) of Pd$_2$(dba)$_3$, and 22 mg (0.046 mmol, 2 mol %) of Pd[P(*t*-Bu)$_3$]$_2$. 1,4-Dioxane (3 mL) was then added via syringe, followed by 1.14 mL (8.59 mmol) of 4-methylstyrene and 0.80 mL (3.73 mmol) of NCy$_2$Me. The mixture was stirred at 70 °C for 2 h and then quenched by filtering through Celite. The filtrate was precipitated into 100 mL of methanol and filtered, and the solid was redissolved in 5 mL of THF. This solution was then filtered again through Celite to remove any remaining Pd particles and reprecipitated into 100 mL of methanol, and the solids were collected by suction filtration, providing an 85% yield. The recovered crude white powder was recrystallized from ethyl acetate and then *m*-xylene to give 25% yield of purified material.

Synthesis of Tris(trimethylsiloxy)silyldimethylaminostilbene. This material was synthesized using the published procedure.[70]

Synthesis of Cyclotetra[(trimethylsiloxy)(dimethylamino-stilbene)]siloxane. This material was synthesized using the published procedure.[70]

Synthesis of 4-(*N,N*-Dimethylamino)styrene. To a dry 100 mL Schlenk flask under N$_2$ atmosphere were added 4-bromo-*N,N*-dimethylaniline (25.0 mmol, 5.0 g), Pd$_2$(dba)$_3$ (0.38 mmol, 0.343 g), P(*t*-Bu)$_3$ (1.5 mmol, 0.304 g), and cesium fluoride (56 mmol,

8.54 g). 1,4-Dioxane (30 mL) was then added by syringe, followed by 8.1 mL of tributylvinyltin (27.7 mmol). The mixture was stirred at room temperature for 24 h and then quenched by precipitation into the mixture of 50 mL of ethyl acetate and 50 mL of water. The solution was filtered through 1 cm Celite, which was washed with 100 mL of ethyl acetate. Next, 300 mL of a 3.4 wt % H$_3$PO$_4$ solution was added to the solution, and the water phase was separated from the organic phase. The water phase was neutralized by 400 mL of 5% aqueous NaOH, and then 200 mL of diethyl ether was added. The organic phase was washed with 100 mL of water three times and then dried with sodium bicarbonate. The solution was evaporated by rotary evaporation at room temperature and dried *in vacuo* for 4 h, providing 2.68 g (73%) of pale yellow liquid. ^{1}H NMR (CDCl$_3$): δ 7.29 (m, 2H), 6.66 (m, 3H), 5.52 (d, 1H), 5.00 (d, 1H), 2.93 (m, 6H). ^{13}C NMR (CDCl$_3$): δ 150.2, 136.5, 127.1, 126.1, 112.2, 109.2, 40.4.

Synthesis of [Me$_2$NStilbeneSiO$_{1.5}$]$_{6.8}$[PhSiO$_{1.5}$]$_{1.2}$. To a dry 25 mL Schlenk flask under N$_2$ were added 0.50 g (1.80 mmol -I) of [IPhSiO$_{1.5}$]$_{6.8}$[PhASiO$_{1.5}$]$_{1.2}$, 18 mg (0.02 mmol, 1 mol %) of Pd$_2$(dba)$_3$, 19 mg (0.04 mmol, 2 mol %) of Pd[P(*t*-Bu)$_3$]$_2$, and 1.0 g of copper metal. 1,4-Dioxane (10 mL) was then added via syringe, followed by 0.86 g (5.88 mmol) of 4-methylstyrene and 0.42 mL (1.96 mmol) of NCy$_2$Me. The mixture was stirred at room temperature for 48 h and then quenched by filtering through Celite. The filtrate was precipitated into 200 mL of methanol and filtered, and the solid was redissolved in 10 mL of THF. This solution was then filtered again through Celite to remove any remaining Pd particles and reprecipitated into 200 mL of methanol, and the solids were collected by suction filtration.

Synthesis of [Me$_2$NStilbeneSiO$_{1.5}$]$_8$. To a dry 25 mL Schlenk flask under N$_2$ were added 0.50 g (1.80 mmol -I) of [*p*-IPhSiO$_{1.5}$]$_8$, 18 mg (0.02 mmol, 1 mol %) of Pd$_2$(dba)$_3$, 19 mg (0.04 mmol, 2 mol %) of Pd[P(*t*-Bu)$_3$]$_2$, and 1.0 g of copper metal. 1,4-Dioxane (10 mL) was then added via syringe, followed by 0.86 g (5.88 mmol) of 4-(*N,N*-dimethylamino)styrene and 0.42 mL (1.96 mmol) of NCy$_2$Me. The mixture was stirred at room temperature for 48 h and then quenched by filtering through Celite. The filtrate was precipitated into 200 mL of methanol and filtered, and the solid was redissolved in 10 mL of THF. This solution was then filtered again through Celite to remove any remaining Pd particles and reprecipitated into 200 mL of methanol, and the solids were collected by suction filtration.

2.3. Analytical Methods. Gel Permeation Chromatography. GPC analyses were done on a Waters 440 system equipped with Waters Styragel columns (7.8 × 300, HT 0.5, 2, 3, 4) with RI detection using a Waters refractometer and THF as solvent. Polystyrene standards were used for calibration and toluene as reference.

Nuclear Magnetic Resonance. All ^{1}H NMR and ^{13}C NMR samples used CDCl$_3$ or DMSO-*d$_6$*, and the spectra were recorded on a Varian INOVA 400 MHz spectrometer. ^{1}H spectra were collected at 400 MHz using a 6000 Hz spectral width, a relaxation delay of 0.5 s, 30k data points, a pulse width of 38°, and TMS (0.00 ppm) as the internal reference. ^{13}C NMR spectra were collected at 100 MHz using a 25 000 Hz spectral width, a relaxation delay of 1.5 s, 75k data points, a pulse width of 40°, and TMS (0.00 ppm) as the internal reference.

Thermogravimetric Analyses. A 2960 simultaneous DTA-TGA instrument (TA Instruments, Inc., New Castle, DE) was used. Samples (15−25 mg) were loaded in alumina pans and ramped at 10 °C/min to 1000 °C under dry air with a flow rate of 60 mL/min.

Differential Scanning Calorimetry. DSC was performed using a DSC 2910 calorimeter (TA Instruments, Inc.). The N$_2$ flow rate was 60 mL/min. Samples (5−10 mg) were placed in pans without capping and ramped to the desired temperature at a rate of 10 °C/min. The heat flow difference between the reference blank and the sample pan was recorded.

(69) Roll, M. F.; Asuncion, M. Z.; Kampf, J.; Laine, R. M. *ACS Nano* **2008**, *2*, 320.

(70) (a) Ronchi, M.; Pizzotti, M.; Orbelli Biroli, A.; Macchi, P.; Lucenti, E.; Zucchi, C. *J. Organomet. Chem.* **2007**, *692*, 1788. (b) Ronchi, M.; Pizzotti, M., results to be published elsewhere.

Matrix-Assisted Laser Desorption/Ionization Time-of-Flight Spectrometry. MALDI-TOF analysis was done on a Micromass TofSpec-2E instrument equipped with a 337 nm nitrogen laser in positive-ion reflectron mode using poly(ethylene glycol) as calibration standard, dithranol as matrix, and $AgNO_3$ as ion source. Samples were prepared by mixing solutions of 5 parts matrix (10 mg/mL in THF), 5 parts sample (1 mg/mL in THF), and 1 part $AgNO_3$ (2.5 mg/mL in water) and blotting the mixture on the target plate.

Solvents for Spectroscopic Studies. All UV−vis and photoluminescence (PL) spectra were recorded using freshly distilled solvents that were thoroughly dried using standard drying agents as noted above. The solvents were kept over molecular sieves while in use during the UV−vis and PL experiments to minimize water absorption from the atmosphere.

UV−Vis Spectrometry. UV−vis spectra were recorded on a Shimadzu UV-1601 UV−vis transmission spectrometer. Samples were dissolved in the required solvent and diluted to a concentration $(10^{-3}-10^{-4}$ M) where the absorption maximum was <10% for a 1 cm path length.

Photoluminescence Spectrometry. Photoluminescent spectra were recorded on a Fluoromax-2 fluorimeter in the required solvent using 320 nm excitation. Samples from UV−vis spectroscopy were diluted $(10^{-5}-10^{-6}$ M) to avoid excimer formation and fluorimeter detector saturation.

Quantum Efficiency. Photoluminescence excitation (PLE) was determined by a modification of the relative method described by Demas and Crosby using anthracene and 1,10-diphenylanthracene as references.[71] The absorption at 320 nm was determined for each material at three different concentrations (maximum absorption of 20%). These samples were then diluted by equal amounts in order to avoid fluorimeter saturation and excimer formation, and the total area of the emission spectrum was calculated. For each solution, absorption and emission measurements were repeated a minimum of two times and averaged. The slope of a plot of emission versus absorption was determined for each material, and relative quantum efficiency was calculated according to the equation

$$\Phi_{PL(x)} = (A_s/A_x)(F_x/F_s)(n_x/n_s)^2 \Phi_{PL(s)}$$

where x is the sample to measured, s the reference, A the absorption at the excitation wavelength, F the total integrated emission, n the refractive index of the solvent, and Φ_{PL} the quantum yield.

Two-Photon Studies. a. Steady-State Measurements. All compounds were used as received without any further purification. They were dissolved in dry THF (see above; Sigma-Aldrich, spectrophotometric grade) for optical measurements. Their absorption spectra were measured using an Agilent (model 8341) spectrophotometer. In order to measure the molar extinction coefficients, the original stock solutions were diluted to 10^{-6} M. The fluorescence spectra were acquired using a Spex-fluorolog spectrofluorimeter. The quantum yields of the molecules were measured using a known procedure.[72] Coumarin 307 (7-ethylamino-6-methyl-4-trifluoromethylcoumarin) was used as the standard.

b. Two-Photon Excited Fluorescence Measurements. In order to measure the two-photon absorption (TPA) cross sections, we used the two-photon excited fluorescence (TPEF) method.[73] A 10^{-4} M Coumarin 307 solution in methanol was used as the reference for measuring TPA cross sections at different wavelengths. The laser used for the study was a Mai Tai diode-pumped mode-locked Ti:sapphire laser. The beam was directed onto the sample cell (quartz cuvette, 0.5 cm path length), and the resultant fluorescence

was collected in a direction perpendicular to the incident beam. A 1-in. focal length plano-convex lens was used to direct the collected fluorescence into a monochromator. The output from the monochromator was coupled to a photomultiplier tube. The photons were converted into counts by a photon counting unit. A logarithmic plot between collected fluorescence photons and input intensity gave a slope of 2, ensuring a quadratic dependence. The intercept enabled us to calculate the TPA cross sections at different wavelengths.

Cathodoluminescent Spectrometry. Cathodoluminescent spectra were recorded from silsesquioxane powders loaded into an ultrahigh-vacuum chamber $(<10^{-9}$ T). Samples, 1-mm thick, were lightly packed in 5-mm-diameter holes in an oxygen-free copper mount and irradiated with a Kimball-Physics EGPS-12B electron gun operated in gate-controlled mode for optimum stability and reproducibility at low currents. An accelerating voltage of 4 kV was used at a current of 5 μA, and the beam was only lightly focused to a diameter of 1 mm at the sample to avoid thermal damage. A Faraday cup was used for current calibration. UV−vis spectra were acquired through a UV-transmitting CaF_2 chamber window with a fiber-coupled EPP2000 spectrograph from StellarNet containing an integrated charge-coupled device detector. Signalto-noise ratios exceeding 20 were attained over acquisition periods as short as 30−120 s. This made it possible to avoid a pronounced bleaching effect that accompanied electron irradiation longer than 5 min and to record emission spectra across the entire UV−vis range.

2.4. Theoretical Methods. All of the calculations reported herein were carried out using the nonlocal gradient corrected density functional theoretical calculations as implemented in the Amsterdam Density Functional Theory program, ADF.[74]

A series of calculations were carried out on each of the different organic-substituted silsesquioxane molecules in order to determine their electronic structure and the specific atomic states which make up the frontier molecular orbitals and their corresponding energies. This information is used to evaluate the electronic transitions associated with light absorption and emission behavior. The Becke−Perdew[75,76] form of the Generalized Gradient Approximation was used to determine the gradient corrections to exchange and correlation energies, respectively. Triple-zeta basis sets were used with two polarization functions (TZ2P) to describe the electronic structure. Relativistic effects are accounted for using the ZORA approach.[77,78] The electronic structures were converged to within 1×10^{-4} eV, whereas the geometries for each of the OPS structures were optimized to within 1×10^{-3} eV. The molecular orbitals along with their corresponding energies for all of the optimized substituted phenylsilsesquioxane molecules were examined to determine the potential charge-transfer states. HOMO−LUMO gaps and electron density maps provided further insight into the electronic transitions.

3. Results and Discussion

In the following sections we first characterize the individual compounds synthesized per the experimental section, thereafter we present the photophysical data and then the theoretical modeling results as a prelude to discussions about the interpretation of this photophysical data. It is also important to describe our efforts to avoid collecting data from the wrong materials as discussed in this latter section.

(71) (a) Demas, J.; Crosby, G. *J. Phys. Chem.* **1971**, *75*, 991. (b) *Standards for Fluorescence Spectrometry*; Miller, J. N., Ed.; Chapman and Hall: London, 1981. (c) Hamai, S.; Hirayama, F. *J. Phys. Chem.* **1983**, *87*, 83.

(72) Maciejewski, A.; Steer, R. P. *J. Photochem.* **1986**, *35*, 59.

(73) Xu, C.; Webb, W. W. *J. Opt. Soc. Am. B* **1996**, *13*, 481.

(74) te Velde, G.; Bickelhaupt, F. M.; Baerends, E. J.; Fonseca Guerra, C.; van Gisbergen, S. J. A.; Snijders, J. G.; Ziegler, T. *J. Comput. Chem.* **2001**, *22*, 931. *ADF SCM*; Theoretical Chemistry, Vrije Universiteit: Amsterdam, The Netherlands, 2001; http://www.scm.com.

(75) Becke, A. D. *Phys. Rev. A* **1988**, *38*, 3098.

(76) Perdew, J. P.; Wang, Y. *Phys. Rev. B* **1986**, *33*, 8822.

(77) Wolff, S. K.; Ziegler, T. *J. Chem. Phys.* **1998**, *109*, 895.

(78) Wolff, S. K.; Ziegler, T.; van Lenthe, E.; Baerends, E. J. *J. Chem. Phys.* **1999**, *110*, 7689.
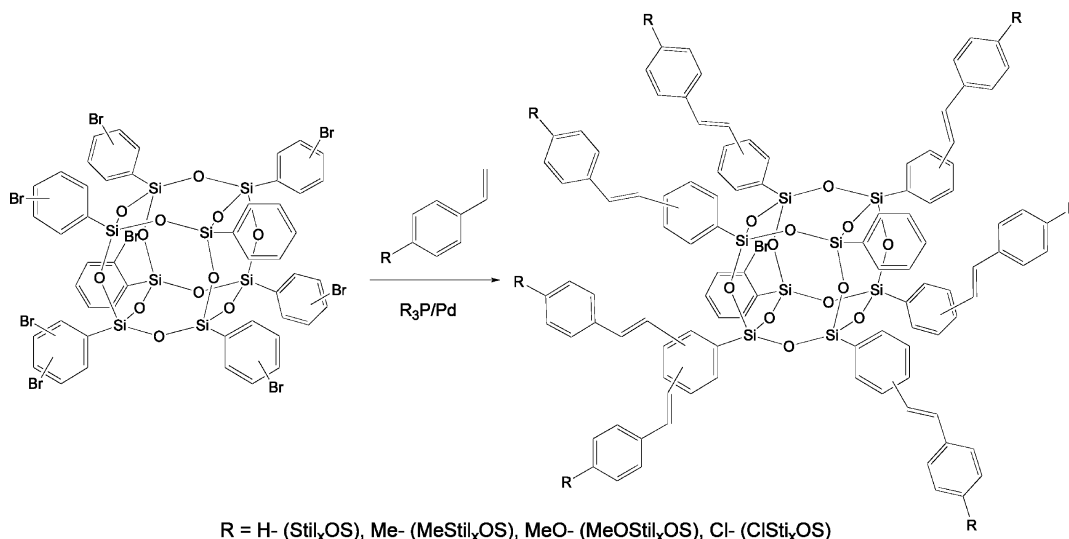
R = H- (Stil$_x$OS), Me- (MeStil$_x$OS), MeO- (MeOStil$_x$OS), Cl- (ClStil$_x$OS)

Figure 1. Synthesis of (RStil)$_x$(Ph)$_{8-x}$OS from (BrPh)$_x$(Ph)$_{8-x}$OS.

Table 1. GPC, TGA, and MALDI-TOF Data for (BrPh)$_x$(Ph)$_{8-x}$OS and (RStil)$_x$(Ph)$_{8-x}$OS Compounds[28]

		compound				
		(BrPh)$_x$(Ph)$_{8-x}$OS	(Stil)$_x$(Ph)$_{8-x}$OS	(MeStil)$_x$(Ph)$_{8-x}$OS	(MeOStil)$_x$(Ph)$_{8-x}$OS	(ClStil)$_x$(Ph)$_{8-x}$OS
GPC	M_n	1009	1330	1669	1667	1756
	M_w	1040	1404	1786	1771	1864
	PDI	1.03	1.06	1.07	1.06	1.06
TGA	ceramic yield, %	31.0	29.2	27.0	27.0	24.0
	theor yield, %	31.9	29.1	27.8	26.3	26.0
	$T_{d5\%}$, °C	460	414	404	401	420
MALDI-TOF	mass ($X = 6$)	1499.5	1644.3	1728.4	1824.4	1848.1
	X_{av}	5.7	6.0	5.8	5.9	5.5

3.1. Synthesis and Characterization of RStilbene$_x$OS. In an earlier paper, we described the synthesis of a series of (BrPh)$_x$(Ph)$_{8-x}$OS compounds including (BrPh)$_{5.3}$(Ph)$_{2.7}$OS,[28] which was used as the starting point for the synthesis via Heck coupling of a *p*-methylstilbene derivative. In this paper, we extend our efforts to synthesize a series of *para*-substituted stilbene derivatives. Here we used a (BrPh)$_{5.7}$(Ph)$_{2.3}$OS, where 5.7 indicates the average degree of Br substitution on the cage (Figure 1). These derivatives were characterized by GPC, TGA, and MALDI-TOF as listed in Table 1. MALDI-TOF data for parent (BrPh)$_{5.7}$(Ph$_{2.3}$)OS and the stilbene derivative are presented in Figure S1 (Supporting Information).

Table 1 data and Figure S1 suggest that the product substitution patterns are identical with the original bromine distribution, with no cage breakdown under the reaction conditions. Likewise, TGA ceramic yields (to SiO$_2$) of the (*p*-RStil)$_{5.7}$(Ph)$_{2.3}$OS products are close to theory, also suggesting quantitative conversion to the desired products. Decomposition onset temperatures ($T_{d5\%}$/TGA/air) for all materials are >400 °C, indicating very robust behavior.

In our previous studies, we determined that the (BrPh)$_{5.3}$(Ph)$_{2.7}$OS averaged 64% *para*-substituted, 24% *meta*-substituted, 9% *ortho*-substituted, and 3% disubstituted compounds.[28] With our recent discovery of a synthetic route to *p*-I$_8$OPS with >99% monoiodination and >95% *para*-substitution,[69] we decided to synthesize the stilbene and methylstilbene derivatives for comparison. In addition, we also purposely synthesized a material with less than I$_8$ average substitution to assess specific photophysical behavior as discussed below. Finally, for reasons discussed in the section on photophysical properties, we also prepared a set of dimethylaminostilbene

compounds including the monomer and tetramer shown in Figure 2. Table 2 offers comparative data for the (*p*-IPh)$_x$(Ph)$_{8-x}$OS-derived stilbene compounds. Representative MALDI-TOF spectra and TGAs are provided as Figures S2−S8, and NMR data are provided in Table S1 (Supporting Information).

In general, the Table 2 data suggest that the new materials are well behaved and mirror the data presented in Table 1. Most important is that F$^-$-promoted cleavage of the Si−C bonds of the starting (*p*-IPh)$_x$(Ph)$_{8-x}$OS compounds[69] reveals only traces of diiodobenzene, indicating that contributions from distyrenylbenzene groups on the SQs to their photophysical properties should be minimal, which is quite important as discussed below.

3.2. Photophysics of (*p*-RStilbene)$_{5.7}$(Ph)$_{2.3}$OS from (Br)$_{5.7}$(Ph)$_{2.3}$OS. Figure 3 provides UV−vis absorption spectra (THF) for the (*p*-RStil)$_{5.7}$(Ph)$_{2.3}$OS listed in Table 1 plus *trans*-stilbene and the model compound *p*-MeStilSi(OEt)$_3$. The UV−vis spectra of (*p*-RStil)$_{5.7}$(Ph)$_{2.3}$OS compounds are all red-shifted 5−10 nm from those of stilbene and the model compound. Normally, it would be reasonable to argue that the effect of the cage on the UV−vis spectra of the attached stilbenes is small. However, it has been suggested in the literature that the −Si(O)$_3$ unit exhibits the inductive characteristics of a −CF$_3$ group.[79] Thus, a blue-shift would be a more reasonable expectation.

In contrast to the mundane UV−vis behavior, the emissive behavior is quite striking. As can be seen in Figure 4, the

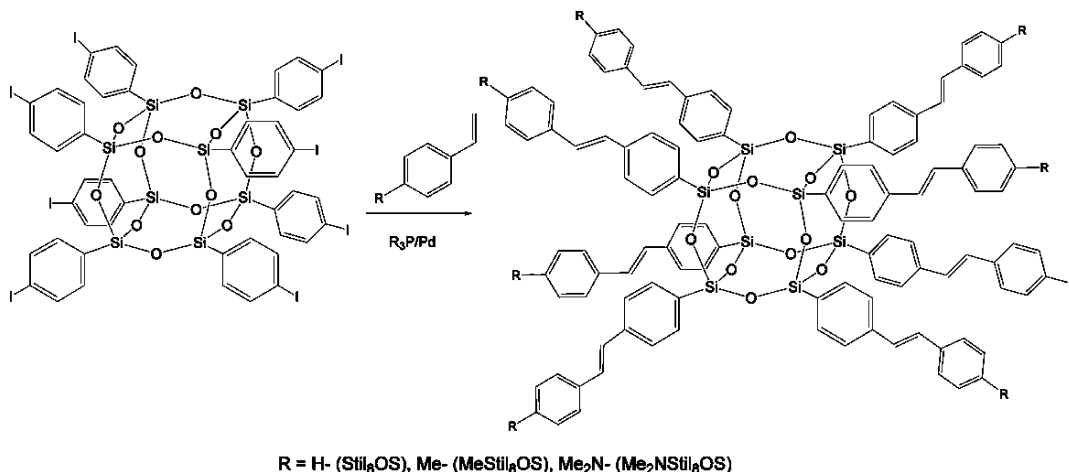(79) Feher, F. J.; Budzichowski, T. A. *J. Organomet. Chem.* **1989**, *379*, 33.

Figure 2. Synthesis of RStil₈OS from I₈OPS.

R = H- (Stil₈OS), Me- (MeStil₈OS), Me₂N- (Me₂NStil₈OS)

Table 2. GPC, TGA, and MALDI-TOF Data for *p*-IPh$_x$Ph$_{8-x}$OS, *o*-Br₈OPS, Selected (*p*-RStil)$_x$(Ph)$_{8-x}$OS Compounds, and *o*-MeStil₈OS

		compound					
		(IPh)$_{6.4}$(Ph)$_{1.6}$OS	Stil₈OS	MeStil₈OS	*o*-MeStil₈OS	Me₂NStil₈OS	(Me₂NStil)$_{6.3}$(Ph)$_{2.7}$OS
GPC	M_n	918	1609	1852	1201	2010	1797
	M_w	929	1641	2007	1217	2048	1873
	PDI	1.01	1.02	1.08	1.01	1.02	1.04
TGA	ceramic yield, %	24.0	26.3	26.3	25.9	21.5	24.1
	theor yield, %	25.1	26.0	24.5	24.5	21.9	23.4
	$T_{d5\%}$, °C	429	410	429	404	325	318
MALDI-TOF	mass ($X = 8$)	2022 (Ag⁺, $x = 7$)	1958 (Ag⁺)	2071 (Ag⁺)	2069 (Ag⁺)	2193 (H⁺)	2050 (H⁺, $x = 7$)
	X_{av}	6.4	8	8	8	8	6.3
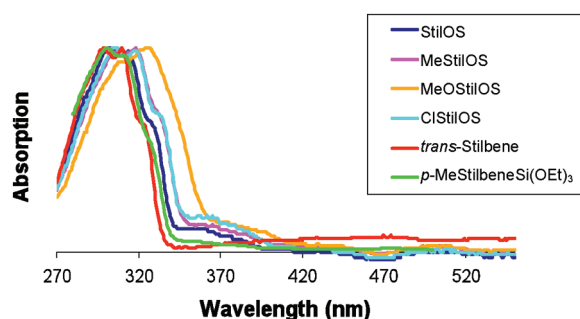
Figure 3. (*p*-RStil)$_{5.7}$(Ph)$_{2.3}$OS and model compound UV−vis spectra (THF). Absorptions normalized to 1.
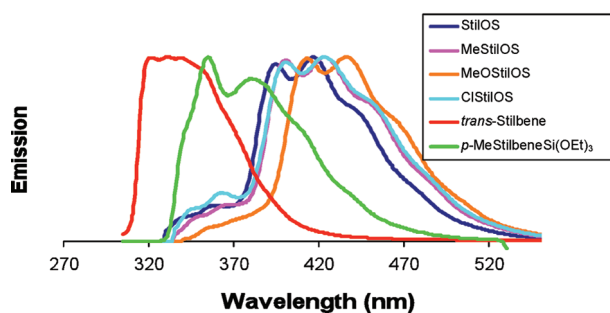
Figure 4. PL spectra of (*p*-RStil)$_{5.7}$(Ph)$_{2.3}$OS and model compounds in THF. Emissions normalized to 1.

emission spectra (normalized) show a red-shift of 60−100 nm or about 0.60−80 eV for all RStil$_{5.7}$Ph$_{2.7}$OS compounds, depending on what maxima are used (see Table 3), relative to those of *trans*-stilbene itself, as discussed below. The individual

(*p*-RStil)$_{5.7}$(Ph)$_{2.7}$OS emission shifts mirror the UV−vis absorption shifts of 5−10 nm seen for the various substituents.

In an effort to explain this significant red-shift, we prepared the model compound *p*-MeStilSi(OEt)₃.[80] This compound exhibits a UV−vis spectrum similar to those seen in Figure 1, while the corresponding emission spectrum is red-shifted partway toward those of (*p*-RStil)$_{5.7}$(Ph)$_{2.3}$OS, indicating some influence of the Si(OEt)₃ group on the LUMO. However, the much greater shifts wrought by attachment to the [SiO$_{1.5}$]₈ or OS core seem inconsistent with attachment to an insulating silica cage with a band gap of 6−7 eV, as suggested by initial modeling studies.

3.3. Photophysics of RStil$_x$OS from I₈OPS and (*p*-IPh)$_{6.4}$(Ph)$_{1.6}$OS. Figure 5 provides UV−vis absorption and PL behavior for Stil₈OS and *p*-MeStil₈OS synthesized from I₈OPS. The UV−vis spectra are very similar to those for (*p*-RStil)$_{5.7}$(Ph)$_{2.3}$OS synthesized from (BrPh)$_{5.7}$(Ph)$_{2.3}$OS. The emission spectra show slightly different patterns and emission maxima compared to the emission spectra of (*p*-RStil)$_{5.7}$(Ph)$_{2.3}$OS: RStil₈OS shows a more structured emission pattern rather than the broad spectra observed for (*p*-RStil)$_{5.7}$(Ph)$_{2.3}$OS, and the emission maxima for RStil₈OS are 15−20 nm blue-shifted from those of (*p*-RStil)$_{5.7}$(Ph)$_{2.3}$OS (see Table 4). These differences arise from the presence of small amounts of dibromophenyl functionality, leading to small amounts of distyrenylbenzene in these SQs as discussed at the end of the paper, under the section headed Other Possible Explanations of the Current Observations.

The absence of diiodophenyl groups in *p*-I$_{6.7}$OPS and *p*-I₈OPS permits a clearer understanding of the photophysical behavior of the stilbene$_x$OS system. The UV−vis absorption spectrum

(80) Cerveau, G.; Chappellet, S.; Corriu, R.; Dabiens, B. *J. Org. Chem.* **2001**, *626*, 92.

**Table 3.** Absorption and Emission Spectra for $(p\text{-RStil})_{5.7}(Ph)_{2.3}OS$

	lowest energy			maxima			0.5FWHH		
compound	abs (nm)[a]	em (nm)[a]	Δnm (eV)	abs (nm)[a]	em (nm)[a]	Δnm (eV)	abs (nm)	em (nm)	Δnm (eV)
$(Stil)_{5.7}(Ph)_{2.3}OS^b$	323	394	70 (0.69)	298	420	122 (1.2)	304	420	116
$(p\text{-MeStil})_{5.7}(Ph)_{2.3}OS^b$	337	402	65 (0.59)	320	424	104 (0.95)	308	427	119
$(p\text{-MeOStil})_{5.7}(Ph)_{2.3}OS^b$	346	412	66 (0.57)	324	436	112 (0.98)	315	444	129
$(p\text{-ClStil})_{5.7}(Ph)_{2.3}OS^b$	337	402	65 (0.59)	306	424	118 (1.3)	308	427	119
$MeStilSi(OEt)_3^c$	329	342	12 (0.14)	298	352	54 (0.64)	304	379	75
trans-stilbene[c]	325	320	0 (0)	306	334	28 (0.34)	303	345	40

^{a} ±5 nm. ^{b} 320 nm excitation. ^{c} 270 nm excitation.
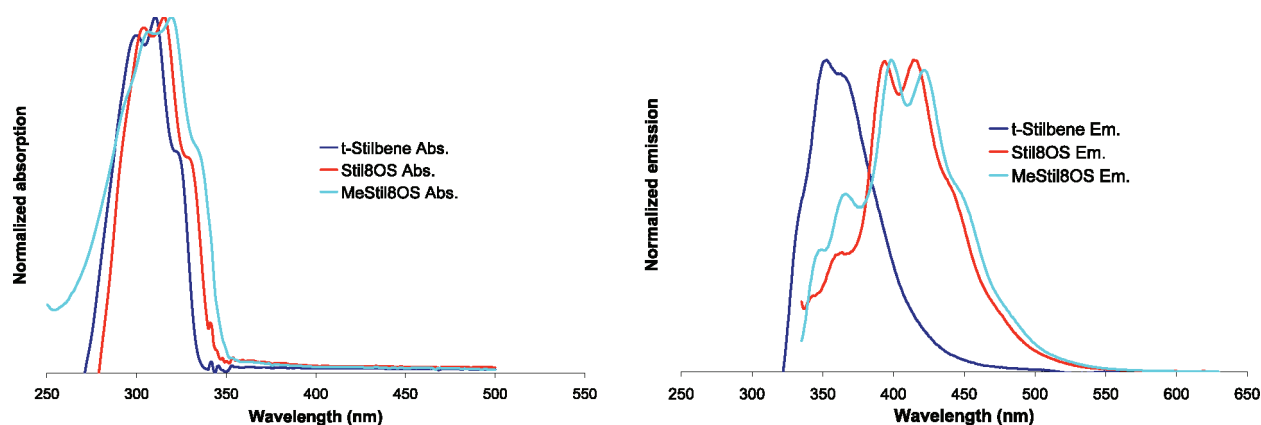
Figure 5. UV−vis absorption and PL emission spectra of *trans*-stilbene and RStil₈OS in THF.

Table 4. Absorption and Emission Maxima for $(p\text{-RStil})_x(Ph)_{8-x}OS$

compound	abs (nm)[a]	em (nm)[a]	Δnm (eV)
trans-4-methyl stilbene	298, 312	352	50
$(Stil)_{5.7}(Ph)_{2.3}OS^b$	298	420	122
$(p\text{-MeStil})_{5.7}(Ph)_{2.3}OS^b$	320	424	104
$p\text{-Stil}_8OS^b$	315	393, 414	78, 99
$(p\text{-MeStil})_7(Ph)OS^b$	319	365	46
$p\text{-MeStil}_8OS^b$	320	400, 422	80, 102
$o\text{-MeStil}_8OPS$	304	402, 426	98, 122

^{a} ±5 nm. ^{b} 320 nm excitation.
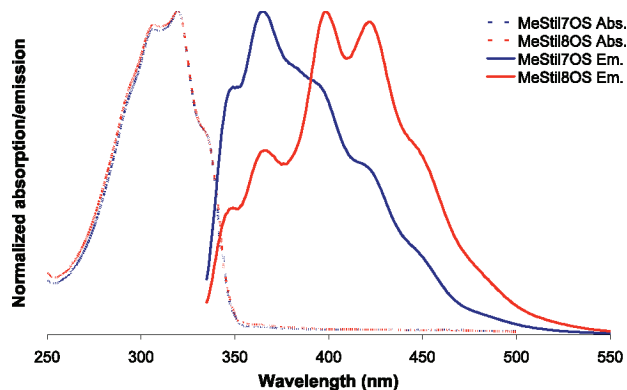
Figure 6. UV−vis absorption and PL spectra of $(p\text{-MeStil})_x(Ph)_{8-x}OS$ in THF.

of $(p\text{-MeStil})_7(Ph)OS$ [actually $(p\text{-MeStil})_{6.7}Ph_{1.3}OS$] is identical to that of $p\text{-MeStil}_8OS$, while the PL spectrum is similar to that of $p\text{-MeStil}_8OS$ with several important differences (see Figure 6). The general shape of the emission spectrum of $(p\text{-MeStil})_7(Ph)OS$ mirrors that of $MeStil_8OS$. However, the intensities of the different emission peaks are much lower at wavelengths higher than 380 nm, suggesting that emissions at higher wavelengths (lower energies) come from having stilbene units at all corners of the silsesquioxane cage.

It appears that the asymmetry brought on by having one or two phenyls on the cage changes the emission structure and possibly the LUMO. Clearly the emission comes from a higher energy and perhaps more localized orbital possibly associated with the phenyl groups, although the normal emission from OPS (THF) is near 290 nm.

In addition to our work here on the cage stilbene systems, Peetz et al. recently developed an ADMET synthesis of cyclic and linear -[stilbene-R_2Si-O-R_2Si]$_n$- compounds.[81] Their results seem to corroborate our findings here. They observe that the UV−vis absorptions (hexane) of the cyclics are essentially the same as those of *trans*-stilbene. However, all emissions are red-shifted 15−20 nm vs those of *trans*-stilbene, with reported maxima near 360 nm looking similar to the spectrum of $(p\text{-}MeStil)_7(Ph)OS$. However, none of these compounds shows the shifts we observe for the $p\text{-MeStil}_8OS$ with maxima ≥400 nm.

Still further evidence comes from the UV−vis behavior of $o\text{-MeStil}_8OS$, which we recently synthesized.[82] Characterization data for this compound are given in Tables 2 and 4, with UV−vis and emission spectra presented in Figure 7. In this instance, the red-shift is still more pronounced than in the other examples. Additional studies done to corroborate the novel excited-state properties of these cage compounds are presented in the next sections.

3.4. Photophysics of $[Me_2NStilbeneSi(OSiMe_3)_3$, Me_2N-corner], $[Me_2NStilbeneSi(O)(OSiMe_3)]_4$, Me_2N-half], and $[Me_2NStilbeneSi\text{-}(OSiMe_3)O_{1.5}]_8$, Me_2NStil_8OS. Ronchi et al. recently described the second-order nonlinear optical (NLO) behavior of siloxane and cyclotetrasiloxane compounds[70] that are equivalent to corner units and halves of the silsesquioxane cage. We obtained samples of these materials and studied their photophysical properties to compare with the octameric silsesquioxane equivalent. Their structures are shown in Figure 8.

(81) Mukherjee, N.; Peetz, R. M. *Macromolecules* **2008**, *41*, 6677.

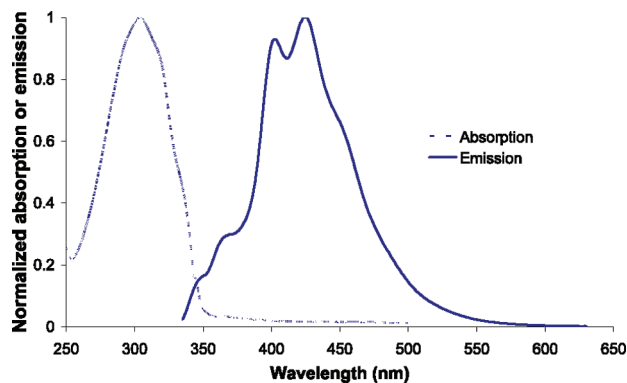(82) Roll, M.; Kampf, J.; Laine, R. M., unpublished work.

Figure 7. UV−vis absorption and PL spectra of *o*-MeStil₈OS in THF.

Figure 9. UV−vis absorption and PL spectra of Me₂NStil-corner and Me₂NStil-half in THF.

Table 5. Absorption and Emission Spectra for Me₂NStil Derivatives

| | solvent | | | | | | | |
| | CH_2Cl_2 | | THF | | 20% THF/80% CH_3CN | | CH_3CN | |
compound	abs[a]	em[a]	abs[a]	em[a]	abs[a]	em[a]	abs[a]	em[a]
Me₂NStil-corner[b]	354	446	348	445	353	461	353	463
Me₂NStil-half[b]	355	454	350	451	350	470		
Me₂NStil₇OS[b]	352	457	349	455			349	477
Me₂NStil₈OS[b]	357	463	356	459	345	475	348	478

[a] ±5 nm. [b] 320 nm excitation. All absorption and emission data given as full width with half-maximum, 0.5FWHM.

Figure 9 shows the UV−vis absorption and PL spectra of Me₂NStil-corner and Me₂NStil-half in THF solutions. Their absorption and emission spectra are, within the limits of the method of analysis, identical (see Table 5). Normally we would expect Me₂NStil-half to show red-shifts in both the absorption and emission spectra. Ronchi et al. attributed the slight blue-shift in the absorption spectrum of Me₂NStil-half to the "very weak π−π interactions between the aromatic rings directly linked to the cyclotetrasiloxane rings."[70] Note that if the Calzaferri concept of conjugation though edge Si−O−Si bonds were correct, we might expect to see some effect with the half-cage, which is not observed.[51]

The photoluminescence quantum efficiency of Me₂NStil-corner is 4%, while that for Me₂NStil-half is 3%. The broad emission spectra and low quantum efficiencies of these compounds suggest charge-transfer processes occurring in these systems, with Me₂NStil-half having more charge-transfer characteristics because its structure includes a larger number of conjugated groups bound together in a smaller volume. To assess this possibility, we measured the UV−vis and PL behavior of these compounds in solvents with different polarities.

The influence of solvent polarity on the UV−vis and PL spectra of Me₂NStil-corner and Me₂NStil-half is shown in Figures 10 and 11, respectively, and summarized in Table 5. Three solvent systems were chosen for this study: CH_2Cl_2, THF, and a mixture of 20% THF and 80% CH_3CN (v/v). CH_2Cl_2 and THF have similar polarities, and we do not expect their spectra to display significant differences. We do expect a shift in the spectra of compounds dissolved in CH_3CN due to its more polar nature.

However, (*p*-Me₂NStil)₇(Ph)OS and Me₂NStil₈OS are only very slightly soluble in CH_3CN due to the polarity of the solvent. Even in very pure materials with <1% impurities, these impurities could have much higher solubilities than the major
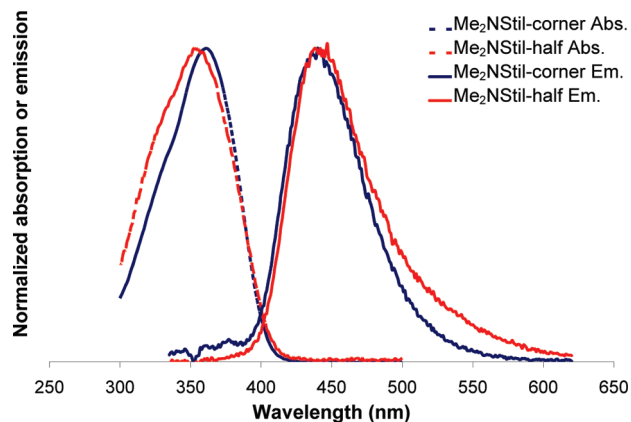
compound; therefore, using solutions where this impurity becomes the major soluble component would result in reporting spectra of the wrong material. By using a mixture of 20% THF and 80% CH_3CN, we were able to ensure that the compounds were completely soluble in the solvent system of interest, and even if there were impurities, they would contribute only in a minor fashion to the UV−vis and PL spectra. Thus, most of our discussions are focused on spectra obtained from these solutions rather than those obtained from 100% CH_3CN solutions.

The UV−vis absorption and PL spectra of Me₂NStil-corner are almost identical when the solvent is changed from THF to CH_2Cl_2, as expected, due to the similar polarity of these two solvents (Figure 10). The same phenomenon is observed for Me₂NStil-half (Figure 11). The absorption spectra of these two compounds do not exhibit any shifts when the compounds are dissolved in 20% THF/80% CH_3CN mixture, while the emission spectra of both compounds show a red-shift of ∼10 nm. We expected Me₂NStil-half to show a larger red-shift in the emission spectrum from our hypothesis that this compound has larger
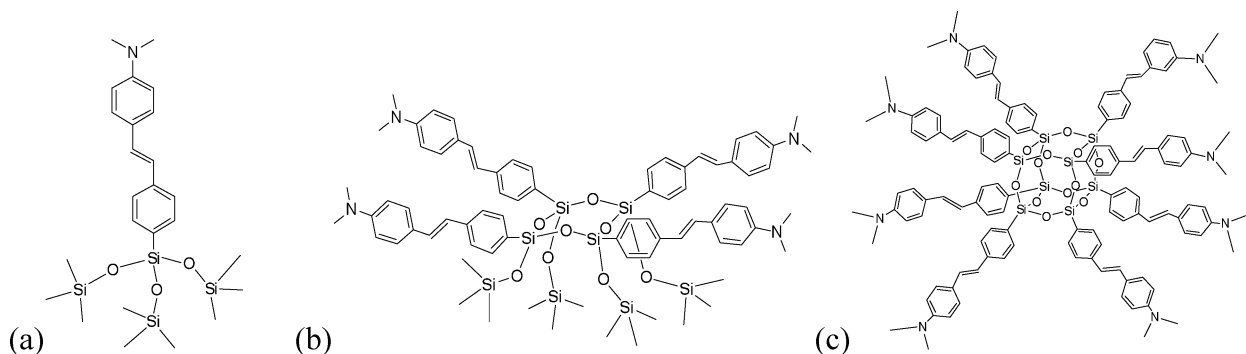

Figure 8. (a) Me₂NStil-corner, (b) Me₂NStil-half, and (c) Me₂NStilOS.
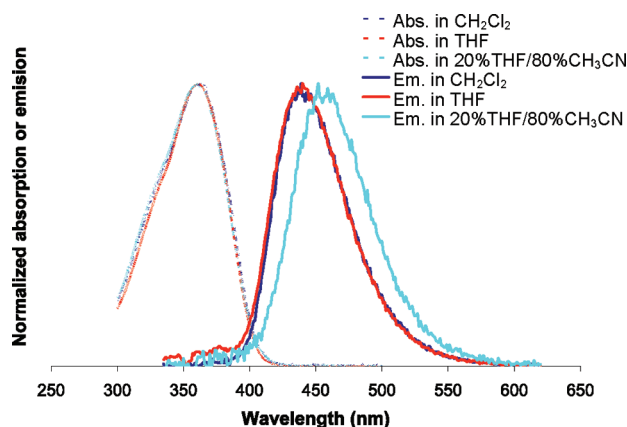
Figure 10. Solvatochromism of Me$_2$NStil-corner in CH$_2$Cl$_2$, THF, and 20% THF/80% CH$_3$CN.
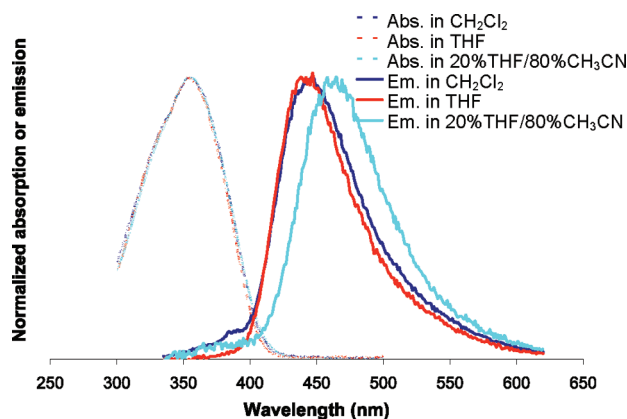

Figure 11. Solvatochromism of Me$_2$NStil-half in CH$_2$Cl$_2$, THF, and 20% THF/80% CH$_3$CN.
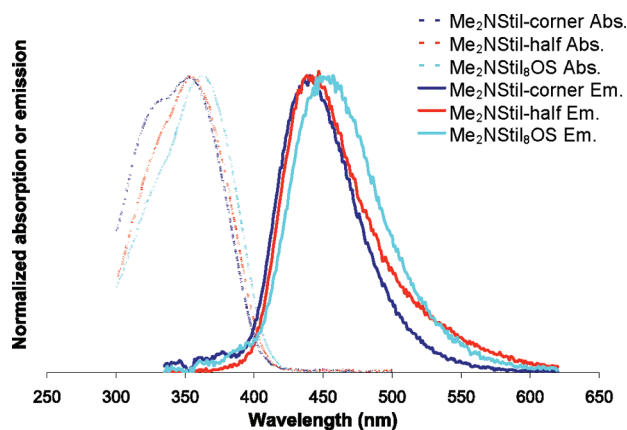
Figure 12. UV−vis absorption and PL spectra of Me$_2$NStil-corner, Me$_2$NStil-half, and Me$_2$NStil$_8$OS in THF.

Figure 13. UV−vis absorption and PL spectra of Me$_2$NStil$_x$OS in THF.
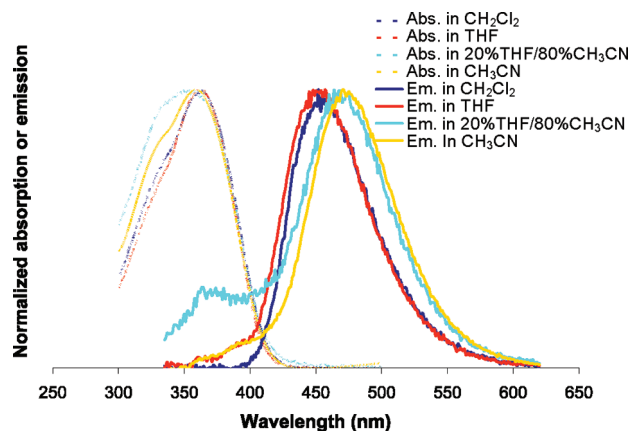
Figure 14. Solvatochromism of Me$_2$NStil$_8$OS in CH$_2$Cl$_2$, THF, 20% THF/80% CH$_3$CN, and CH$_3$CN.

charge-transfer characteristics than Me$_2$NStil-corner. These data provide the basis for a discussion of the photophysical properties of the cage compound.

3.5. Photophysics of (p-Me$_2$NStil)$_x$(Ph)$_{8-x}$OS from (p-IPh)$_{6.3}$-(Ph)$_{1.7}$OS and I$_8$OPS. The UV−vis and PL spectra of Me$_2$NStil-corner, Me$_2$NStil-half, and Me$_2$NStil$_8$OS in THF solutions are plotted in Figure 12. The shapes of both the absorption and emission spectra of Me$_2$NStil$_8$OS are very similar to those of the other two compounds, as expected due to the charge-transfer process observed for these systems. The absorption and emission maxima of Me$_2$NStil$_8$OS are red-shifted by ∼10 nm from the corner and half-cage compounds, although we were expecting
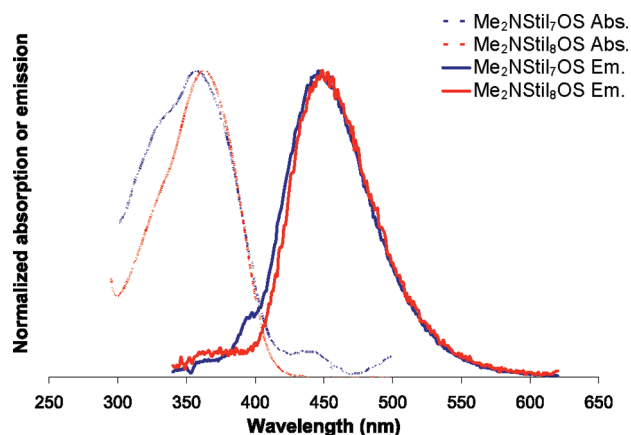
a larger red-shift, considering that this system has a much higher number of conjugated groups.

Figure 13 shows the UV−vis absorption and PL spectra of (p-Me$_2$NStil)$_x$(Ph)$_{8-x}$OS synthesized from (p-IPh)$_7$(Ph)OS and I$_8$OPS. On the basis of our results with (p-MeStil)$_x$(Ph)$_{8-x}$OS (Figure 6), we expected to see significant differences in the PL spectra of (p-Me$_2$NStil)$_x$(Ph)$_{8-x}$OS. However, the PL spectra of these two compounds have almost identical shapes, with only a slight blue-shift observed for (p-Me$_2$NStil)$_7$(Ph)OS. We believe that the charge-transfer characteristics of the dimethylamino-stilbene groups dominate the emission behavior of these compounds.

We also investigated the solvatochromism of (p-Me$_2$NStil)$_x$(Ph)$_{8-x}$OS in solvents with different polarities. For Me$_2$NStil$_8$OS we used four different solvent systems: CH$_2$Cl$_2$, THF, a mixture of 20% THF/80% CH$_3$CN, and CH$_3$CN (see Figure 14). As was seen in the solvatochromism study of Me$_2$NStil-corner and Me$_2$NStil-half, the UV−vis absorption spectra of Me$_2$NStil$_8$OS are almost identical in all solvent systems. The emission spectra in THF and CH$_2$Cl$_2$ are almost identical, while there is a slight red-shift of ∼7 nm in the 20% THF/80% CH$_3$CN mixture. These results mirror those obtained for Me$_2$NStil-corner and Me$_2$NStil-half. The emission spectrum of Me$_2$NStil$_8$OS in CH$_3$CN is red-shifted further, as expected since the polarity of this system is even greater than that of the 20% THF/80% CH$_3$CN mixture.

We also studied the solvatochromism of (p-Me$_2$NStil)$_7$(Ph)OS in three different solvent systems: CH$_2$Cl$_2$, THF, and CH$_3$CN (see Figure S9, Supporting Information). As observed with the

Table 6. Steady-State Properties of Silsesquioxane Derivatives in THF

sample	λ_{abs}, nm	λ_{em}, nm	Φ_f	Stoke's shift $\Delta\nu$, cm^{-1}
(p-MeStil)$_8$OS	317	365	0.06	
Me$_2$NStil-corner	355	445	0.08	5700
Me$_2$NStil-half	361	436	0.09	4760
(p-Me$_2$NStil)$_8$OS	365	454	0.03	5370
NH$_2$StilOVS^a	367	481	0.05	

^{a} Reference 67.

solvatochromism studies of the other Me$_2$NStil-derivatives, the UV−vis spectra of (p-Me$_2$NStil)$_7$(Ph)OS show little change when the compound is dissolved in different solvents. The emission spectra are also almost identical for the THF and CH$_2$Cl$_2$ solutions and are red-shifted for the CH$_3$CN solution, as expected. Perhaps the most important photophysical studies done on the Me$_2$NStil systems are the two-photon cross-section studies discussed in the following section that provide convincing evidence of the significant difference in how these materials respond to light.

3.6. Two-Photon Analyses of Me$_2$NStil-corner, Me$_2$NStil-half, and Me$_2$NStil$_8$OS. Steady-State Measurements. The measured optical absorption and fluorescence spectra of the investigated systems dissolved in THF are shown in Figure S10 in the Supporting Information. A summary of the corresponding optical properties is shown in Table 6; in addition we have added data on the MeStil$_8$OS compound and the [p-NH$_2$PhCH=CHPhCH=CH$_2$SiO$_{1.5}$]$_8$NH$_2$StilOVS compound from our previous paper.[67]

It can be observed from the figure and table that the absorption of the Me$_2$NStil-half is red-shifted in comparison to that of the Me$_2$NStil-corner, and the full cage is red-shifted still further. This might follow the expected trend in increasing wavelength of absorption with length of interaction and conjugation in these particular compounds. However, the emissions of these derivatives show an interesting effect in the Stokes shift. The Me$_2$NStil-corner emission is red-shifted in comparison to that of the Me$_2$NStil-half; furthermore, it also exhibits a greater shift than the full cage. This is contrary to what might be expected, and at this moment we have no explanation for these results.

The fluorescence quantum yield (Φ_f) measurements for these two compounds are also unexpected. First, that of the Me$_2$NStil-corner is smaller than that found for Me$_2$NStil-half, which might be expected; however, the full cage has the lowest Φ_f of all. A number of similar organic chromophoric systems have been investigated in the past. In particular, it was found that the extent of charge separation or transfer in these systems has a dramatic effect on the Stokes shift. This has also been connected to the extent of disorder or conformational rearrangement in the system. The reduction of the quantum yield from Me$_2$NStil-half to Me$_2$NStil-corner is also in accordance with the increased charge-transfer character of the chromophores. In this case, for Me$_2$NStil-corner the extent of charge transfer is reduced by the fact that the system becomes unsymmetrical at the joining points and the charge correlation is lost. This same argument can be used to explain the lowest Φ_f observed for the full cage, suggesting that charge-transfer effects dominate the photophysics of this compound. Consequently, we carried out two-photon measurements on these systems to probe the varying extent of charge correlation in these novel systems.

Two-Photon Absorption Measurements. TPA cross sections as a function of wavelength are plotted in Figure 15 for the Me$_2$N chromophores. The data are presented in Table 7,
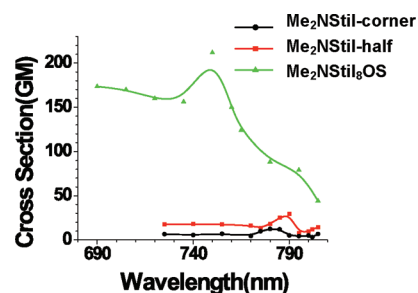
Figure 15. Two-photon absorption cross-section spectra for the investigated chromophores.

Table 7. TPA Properties of Silsesquioxane Derivatives

| sample	δ (GM)	δ/moiety (GM)	λ_{max}, nm
MeStil$_8$OS	11	1.2	735
Me$_2$NStil-corner	12	12	780
Me$_2$NStil-half	30	7.5	790
(p-Me$_2$NStil)$_8$OS	211	26	755
StilOVS^a	25	3	705
MeOStilOVS^a	110	14	705
NH$_2$StilOVS^a	810	101	720

^{a} Reference 67.

including data from our recent paper where conjugation at the cage begins with vinyl rather than phenyl groups.[67] It is clear from the TPA cross sections that the cross section increases with increasing numbers of chromophores. However, the cross section "per chromophore" in these systems is not enhanced by the additional chromophores in the case of Me$_2$NStil-half. The cross section increases by a factor of 2.5, while the number of chromophores increases by 4. This seems to correlate well with the steady-state measurements described above. In the case of Me$_2$NStil-half, while the absorption measurements suggest a red-shift and longer range interaction, the fluorescence and quantum yields suggest a system with lower charge-transfer character.

The TPA (and resulting fluorescence) spectra appear to also follow this trend, as the increase in cross section is found for Me$_2$NStil-half but the enhancement factor observed in a number of different donor−acceptor charge-transfer systems is not present here.[83,84] The degree of conformational flexibility is an effect that we have previously observed to change the long-range nonlinear optical properties in a number of systems. While it appears that these systems could have considerable rigidity across the junctions of the building blocks, small vibrations and conformational changes are just enough to cause disruption of the charge correlation. Further investigations of these effects are underway with time-resolved measurements such as transient absorption and fluorescence upconversion.

Perhaps the most important observations from these studies are the fact that the GM value for the full cage is 26/moiety, whereas the half-cage is 8/moiety and the corner is 12/moiety. The fact that the full cage offers 2−3 times the TPA of the fragments combined with the lowest Φ_f suggests that this system offers much higher charge transfer than the fragments. This type of behavior is more pronounced in the OVS systems studied earlier, which have longer conjugation lengths, as shown in Table 7.[67] However, the data continue to support our contention that in the excited state, the cage seems to influence the

(83) Ramakrishna, G.; Bhaskar, A.; Goodson, T. G. *J. Phys. Chem. B* **2006**, *110*, 20872.

(84) Goodson, T. G. *Acc. Chem. Res.* **2005**, *38*, 99.
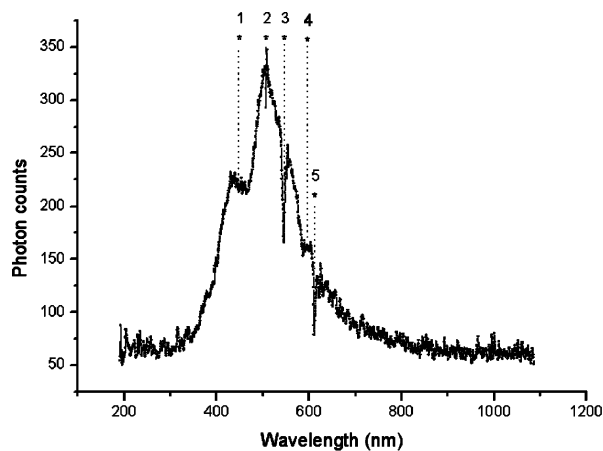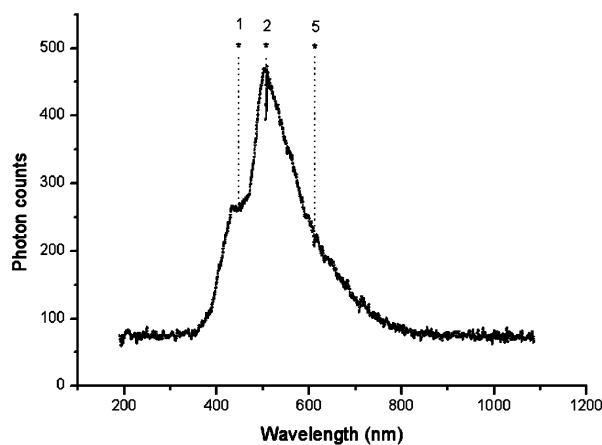
a   b

Figure 16. Cathodoluminescence spectra of MeStil₈OS (a) still contaminated with residual Pd catalyst and (b) after purification with *N*-acetyl-ʟ-cysteine.

Table 8. Absorption Lines of Rare Earth Impurities in (*p*-MeStil)₈OS

peak no.	abs, nm	RE ion	transition state	absorption type[a]
1	447	Er^{3+}	$^4I_{15/2} \rightarrow {}^4F_{5/2}$	GSA
2	506.5	Er^{3+}	$^4I_{13/2} \rightarrow {}^4G_{11/2}$	ESA
3	545.5	Er^{3+}	$^4I_{15/2} \rightarrow {}^4S_{3/2}$	GSA
4	596.7	Pr^{3+}	$^3H_4 \rightarrow {}^1D_2$	GSA
5	614.3	Pr^{3+}	$^3H_6 \rightarrow {}^3P_0$	ESA

[a] GSA, ground-state absorption; ESA, excited-state absorption.

photophysics more than would be expected if each corner served solely as a SiO₃ fragment.

It is important to add at this point that the effect of a simple SiO₃ fragment on the UV−vis and emission behavior of methylstilbene is also much less than seen in the complete cage, per Table 6.

3.7. Cathodoluminescence Spectroscopy. This set of experiments allows us to study the nature of the excited state of MeStil₈OS and its relaxation to the ground state in response to energy transfer via electron bombardment instead of photon absorption. Furthermore, it is done on powder samples rather than in solution, providing a quite different method of assessing the photophysics of these compounds. Cathodoluminescence provides a mechanism to access higher energy states not normally accessible by optical pumping.[85] It also provides an alternate mechanism of accessing the same excited states. Our goal here was simply to confirm that we see the same excited states as seen via optical pumping. However, it is important to note that the relaxation process from higher energy states can populate higher thermal energy states within the lowest excited state, leading to decomposition.

Figure 16 shows the cathodoluminescence spectra of MeStil₈OS at different purity levels. The Figure 16a spectrum was taken from a sample of MeStil₈OS still contaminated with palladium catalyst residues from the Heck synthesis. The spectrum shows strong absorption lines due to trivalent erbium and praseodymium overlying the cathodoluminescence of the host (see Table 8 for detailed information on the rare earth (RE) impurity peaks). These RE emissions arise from minor impurities in the Pd catalyst. Four spots on the sample were tested and displayed very different amounts of the RE impurities. The
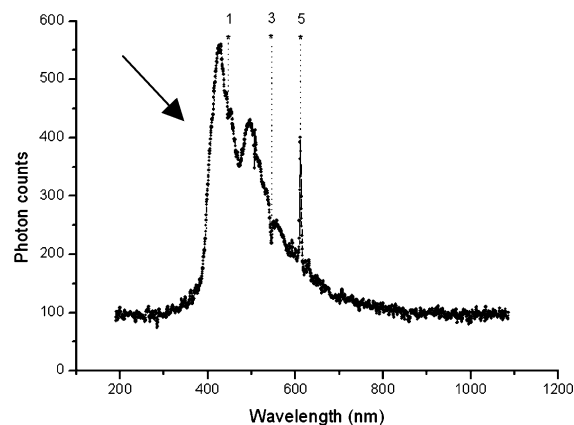
(85) Li, B.; Williams, G.; Rand, S. C.; Hinklin, T.; Laine, R. M. *Opt. Lett.* **2002**, *27*, 394.

Figure 17. Cathodoluminescence spectrum of MeStil₈OS taken at short (<30 s) irradiation times.

RE absorption lines are still present in the cathodoluminescence spectra of MeStil₈OS treated with *N*-acetyl-ʟ-cysteine to remove the residual palladium catalyst (Figure 16b), although at much lower intensities, supporting the likelihood that these impurities come from the Pd catalyst residues from the synthesis. One important note is that the RE impurities have their own distinct absorption lines and do not interfere with the emission of the host material [(*p*-MeStil)₈OS].

Figure 17 shows the cathodoluminescence spectrum of purified MeStil₈OS taken at short (<30 s) irradiation times. The RE absorption lines are at lower intensities than those shown in Figure 16a. The peak at ~425 nm is much more prominent in this spectrum than in the spectra shown in Figure 16. This peak is present in all samples at short (<30s) irradiation time, bleaches quickly under electron excitation, and always leaves a shoulder at 450 nm, as is evident in the spectra shown in Figure 16. The odd shape of this residual shoulder is due to overlapping of erbium absorption lines.

The peak at 425 nm is evidently from a species that is more reactive than the rest of the material in response to electron bombardment. We believe that this emission comes from the (*p*-MeStil)₇(Ph)OS component of this batch of MeStil₈OS, given the similar spectrum seen above in Figure 6. The quite different spectrum for this compound from that of the fully octa-substituted analogue might, as mentioned above, arise from a more localized emission, resulting in higher reactivity and more rapid thermal decomposition.

Table 9. DFT HOMO−LUMO Calculations for Various [XSiO$_{1.5}$][24]

	[HSiO$_{1.5}$]$_8$	[FSiO$_{1.5}$]$_8$	[HOSiO$_{1.5}$]$_8$	[NH$_2$SiO$_1$.]$_8$	OPS	StilSi(OSiMe$_3$)$_3$	Stil$_1$[SiO$_{1.5}$]$_8$	Stil$_8$OS
HOMO (eV)	−7.519 (O)	−8.79 (O)	−7.384 (O$_{cube}$)	−5.747 (N)	−5.529	−5.165	−5.466	−4.519
core/LUMO (eV)	−0.541 (H,Si)	−2.33 (F)	−1.218 (H,Si)	−0.564 (H)	−0.035	−0.213 (SiO3)	−0.406	−0.293
organic/LUMO (eV)					−0.865	−2.461	−2.767	−1.906
core gap (eV)	6.978	6.46	6.166	5.183	5.564	4.95	5.056	4.79
organic gap (eV)					4.664	2.70	2.695	2.613

Pr^{3+} also appears as line 5 in Figure 17. Its presence in emission rather than as an absorption feature, in combination with Er^{3+} excited absorption from ^{4}I$_{13/2}$, suggests that host excitation by energetic electrons leads to emission from the methylstilbene groups, but also excites Pr^{3+} emission by connecting to this impurity via its high-lying ^{1}S$_0$ state near or in the host conduction band. During the relaxation of the Pr^{3+}, energy transfer to the Er ^{4}I$_{13/2}$ state takes place and accounts for excited-state absorption by this second RE impurity species.

An additional observation with the cathodoluminescence data is that emission from these materials is further red-shifted than for the optically pumped materials. The emission looks closer to that for the (*o*-MeStil)$_8$OS.

Given that the Pd catalysts used here are supposedly homogeneous under the reaction conditions, it is surprising to find REs in these systems. It may be that some small nanoparticles of Pd/RE solid solutions are present in the catalyst precursor(s) and may be resistant to the chemical reactions that lead to formation of the soluble forms of these materials, e.g., Pd$_2$(DBA)$_3$ or Pd(*t*-Bu$_3$P)$_2$.

3.8. Theoretical Studies. Calzaferri, in theoretical studies of electron transfer between napthyl and biphenyl groups bound to octasilsesquioxanes via vinyl groups, noted that the properties of siloxane bridges in these octasilsesquioxanes range from insulating to conducting.[51] We have also observed much improved electroluminescence in related vinyl-functionalized silica cores, suggesting that the observed phenomena could be general in nature.[25] Thus, it is possible that the changes observed involve core edges. Given that there are at least six stilbene units per silica core for all the compounds reported here, the bridges will all be relatively similar and, consequently, mostly energetically equivalent, leading to the conclusion that "conducting" behavior, or conjugation, could be 3-D along the edges rather than through the cage.

Modeling studies on [XSiO$_{1.5}$]$_8$ (X = H, F, HO, NH$_2$, etc.) by multiple groups[19–23] and recently by us (see Figure 18 and Table 9) suggest HOMO−LUMO band gaps that range between 5 and 7 eV, typical of insulators. The HOMO involves the 2p lone-pair states on the oxygen atoms, as shown in Figure 18a. The LUMO involves contributions from the 3p states of Si atoms and the organic substituents. The LUMO of the base [HSiO$_{1.5}$]$_8$ system involves all of the Si atoms equally, is roughly spherical,
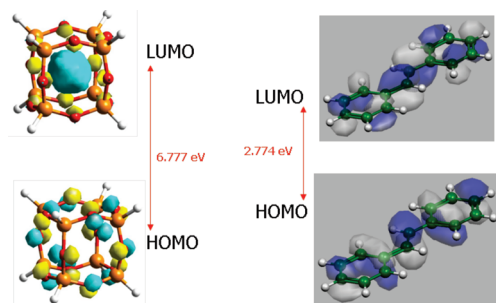
and resides in the center of the core, as shown in Figure 18b. This state, referred to herein as the core state, is highly electrophilic and may be important with respect to the luminescence behavior discussed above.

Our calculations here reveal that the more electron-withdrawing substituents such as F, HO, and NH$_2$ decrease the electron density within the cage and act to lower band gaps of the substituted [SiO$_{1.5}$]$_8$, as shown in Table 9. Functionalization of the core [SiO$_{1.5}$]$_8$ cages with conjugate tethers such as phenyl or stilbene leads to more significant changes, as the HOMO and LUMO states are now the π and π* states that are localized on the organic. The HOMO−LUMO gap decreases in the following order for the octa-functionalized systems presented in Table 9:

$$H\ (6.98\ eV) > phenyl\ (4.66\ eV) > stilbene\ (2.61\ eV)$$

If we focus solely on the influence on the HOMO−LUMO gap of stilbene-functionalized systems (i.e., organic stilbene, molecular, stilbene, trimethylsiloxysilyl stilbene, monostilbeneOS, and octastilbeneOS), however, we find the changes that result are significantly smaller since these states are localized on the π and π* orbitals of stilbene and the corner Si atoms in all of these systems, as shown in Figure 19. There is a small overall decrease of 0.08 eV on moving from the single substituted trimethylsiloxysilyl and the octastilbeneOS. This is consistent with the experimental results, which show very minor changes in the UV spectra.

There appears to be a much greater change, however, in the energy difference between the lowest unoccupied core state of the SQ cage (LUMO+4) and the HOMO (π state on stilbene), which is 0.27 eV on moving from the mono- to octa-functionalized SQ, as reported in the data for the core gap in Table 9. The emissions may result from this state, which is localized inside the cage on the O and Si atoms and contains 4a$_1$ symmetry, as shown in Figure 20. The calculated gaps, however, range between 5.06 and 4.79 eV for the stilbene-functionalized OS.

Figure 18. LUMO and HOMO of [XSiO$_{1.5}$]$_8$ (see Supporting Information).
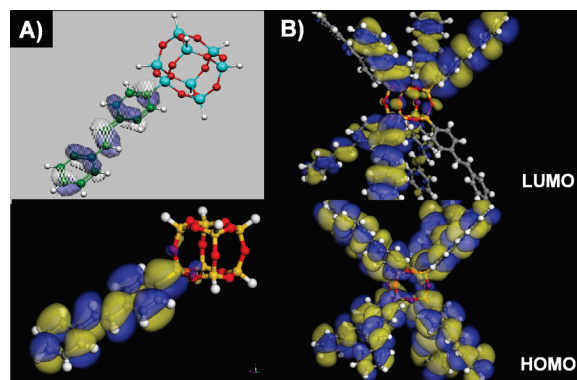

Figure 19. HOMO and LUMO states for (A) mono- and (B) octastilbene-functionalized OS which result from the interaction of states on corner Si atoms with the π (HOMO) and π* (LUMO) states of the stilbene tethers.
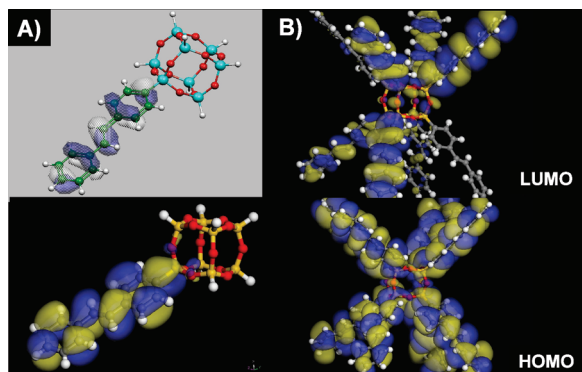
Figure 20. HOMO and LUMO core (LUMO+4) states for (A) mono- and (B) octastilbene-functionalized OS, residing on the stilbene tethers.

Table 10. Solution (THF) Quantum Yields for Various StilbeneOS and Model Compounds

	Φ_f (%)		
compound	for Br$_{5.7}$[a]	for I$_{8.0}$	for I$_{6.3}$
StilOS[b]	37	2	9
MeStilOS[b]	60	4	2
MeOStilOS[b]	38		
ClStilOS[b]	54		
MeStilbeneSi(OEt)$_3$[c]	7		
Trans-Stilbene[c]	5		

[a] Average of relative value to anthracene[70a] and diphenylanthracene.[70b] [b] 320 nm excitation. [c] 270 nm excitation.

It is important to note, however, that the DFT-calculated band gaps can be significantly underestimated. Marsmann et al.[54] have shown that the band gap calculations on the [SiO$_{1.5}$]$_8$ cage are high. They find that all [XSiO$_{1.5}$]$_8$ (where X = CH$_3$, CH$_3$CH$_2$, ..., decyl) absorb 3.8 eV (325 nm) light and emit "blue" light weakly at ∼2.8−3.5 eV (330−370 nm). Even though they calculate a 6.0 eV band gap for [HSiO$_{1.5}$]$_8$, they measure an experimental value of 4.4 eV, which is 1.6 eV lower. Note that the data in Figures 4−14 and Tables 3−8 are obtained on excitation at 320 nm equivalent to the 325 nm (3.8 eV) used by Marsmann.[54] We calculated the HOMO−LUMO band gap for the core [HSiO$_{1.5}$]$_8$ structure at 6.98 eV using ADF as well as time-dependent DFT calculations and at 6.78 using periodic DFT calculations, which are somewhat higher than the value of 6.0 eV calculated by Marsmann et al.[54]

The energy difference, however, between the HOMO and the core (core gap) on this system drops to ∼4.23 eV from the original 7.0 eV. If, as found by Marsmann, the calculated band gaps are 1.6 eV too high for both systems, the actual core-based band gap could then be close to 2.6 eV, roughly the same as that for the stilbenes. Thus, the potential exists for the cage-centered or "core" orbital to be of the same energy as the excited state of the stilbene. If so, then it appears possible to have 3-D conjugation through the core. If correct, then it is not clear if we are exciting the silica core or the stilbene ligands, or both.

Clearly, the behavior is not that expected for simple stilbenes, leading to our conclusions concerning the involvement of a cage-centered LUMO in the excited-state photophysics of these molecules.

3.9. Other Possible Explanations of the Current Observations. We are aware that there are other interpretations that might explain at least some of our results. For example, in our earliest work, we saw very high Φ_f as listed in Table 10. However, as mentioned above, Br$_{5.3}$OPS contains 3% dibrominated compounds. Similarly, (BrPh)$_{5.7}$(Ph)$_{2.3}$OS contains ∼5% dibromi-

nated phenyl groups, providing di-(Rstyryl)phenyl groups upon Heck coupling with *p*-Rstyrene (see Figure 1). These distyrylphenyl groups have longer conjugation lengths and therefore are at lower energies than the stilbene groups.

We believe that all the energy absorbed by the molecule is funneled to these distyrylbenzene groups, giving rise to higher Φ_f as seen in Table 10, larger red-shifts, and much broader emission spectra for (*p*-RStil)$_{5.7}$(Ph)$_{2.3}$OS. This would be one explanation for the extreme red-shifts observed and is the reason we went on to study the I$_8$OPS products, where we have much better control of both the degree of substitution and the point of substitution on the rings. The Φ_f values for these materials, also listed in Table 10, are more in line with those observed for the model compound and *trans*-stilbene. Note that the chloro- and methoxystilbene derivatives were not synthesized from the I$_8$OPS.

As an aside, the great facility with which energy transfer occurs in these small molecules points to their potential utility as antenna structures for organic photovoltaics, etc.[86] Hogen-Esch points out that for cyclic polystyrenes,[86] the smaller the cycle, the more likely the formation of excimers. Hence, we also considered the possibility that the emissions observed here arise from excimers forming in solution. The data reported here were reproduced in two of our collaborating laboratories on two separate instruments at high dilutions to minimize the chance for excimer formation. See, for example, Figure S11 (Supporting Information), taken for the *ortho* compound, where no changes are observed with serial dilutions. Likewise, no changes are observed in emission spectra at high concentrations.

An alternate possible source of the energy transfer could be internal exciplex formation; however, the single-crystal structure of Stil$_8$OS (Figure S12, Supporting Information)[82] suggests that the stilbene moieties are indeed all *para*-substituted and orthogonal to each other. Thus, there appears to be no simple way that they might rotate such that they are in contact with each other, as discussed more below.

Finally, most excimer emissions are broad, without fine structure. In contrast, all of the emissions observed here exhibit fine structure typical of stilbene and styrene compounds.[81,86,87] Indeed, recent work on stilbene π-dimers shows unstructured emissions.[88] Finally, the cathodoluminescence studies indicate that we can access the same excited states by energy injection, and again the emission data are similar to the solution emissions despite the fact that, in the solid state, there is ample opportunity to form exciplexes.

4. Conclusions

In the work reported here, we prepared a series of stilbene-substituted octasilsesquioxane compounds with the average number of stilbenes per [*p*-R-Stil$_x$Ph$_{8-x}$OS]$_8$ cage ranging from $x = 5.3$ to 8. We also synthesized [*o*-MeStil$_x$SiO$_{1.5}$]$_8$ and the corner and half-cages: [*p*-MeStilSi(OEt)$_3$], [*p*-Me$_2$NStilSi(OSiMe$_3$)$_3$], and [*p*-Me$_2$NStilSi(O)(OSiMe)]$_4$.

The full and partial cages all show UV−vis absorption spectra identical to that of *trans*-stilbene, which is consistent with theoretical predictions, which show very small differences in the calculated HOMO−LUMO band gaps. However, the partial

(86) (a) Hogen-Esch, T. H. *J. Polym. Sci. Part A: Polym. Chem.* **2006**, *44*, 2139. (b) Gan, Y.; Dong, D.; Carlotti, S.; Hogen-Esch, T. E. *J. Am. Chem. Soc.* **2000**, *122*, 2130.
(87) Meier, H. *Angew. Chem. Int.* **1992**, *31*, 1399.
(88) Chung, J. W.; You, Y.; Huh, H. S.; An, B.-K.; Yoon, S.-J.; Kim, S. H.; Lee, S. W.; Park, S. Y. *J. Am. Chem. Soc.* **2009**, *131*, 8163.

cages show emissions that are red-shifted by about 20 nm, as found for stilbene−siloxane macrocycles,[76] suggesting some interaction of the silicon center with the stilbene π^* orbital in both the corner and half-cages. In contrast, the full cages show red-shifts of 60−100 nm. These large red-shifts are proposed to result from interactions of the stilbene π^* orbitals with a LUMO centered within the cage that has $4A_1$ symmetry and involves contributions from all Si and oxygen atoms and the organic substituents. Given that this LUMO has 3-D symmetry, it appears that all of the stilbene units interact in the excited state. In the case of the Me$_2$N- derivatives, this interaction is primarily a charge-transfer interaction, as witnessed by the influence of solvent polarity on the emission behavior.[67]

Support for this conclusion comes from several observations. First, the effect of solvent polarity on the emission behavior of the Me$_2$N- derivatives is greatest (26 GM per group) in the full cage system. More importantly, the two-photon absorption behavior is 2−3 times greater per p-Me$_2$Nstilbene for the full cage than for the corner or half-cage. Note that similar observations were made for p-NH$_2$stilbenevinyl$_8$OS cages,[67] where the greater conjugation lengths led to even greater red-shifts (120 nm) and two-photon absorption cross sections of 100 GM per p-NH$_2$Stilvinyl group.

As noted just above, only the emissions are greatly red-shifted in these molecules, whereas the ground-state UV−vis absorptions are not changed from *trans*-stilbene, suggesting that the interactions occur only in the excited state. Furthermore, for the compounds [p-RStil$_{6-7}$Ph$_{2-1}$OS]$_8$, the emissions are blue-shifted compared to those of the fully substituted compounds, suggesting the symmetry is changed, greatly reducing the potential for 3-D delocalization.

One of the reviewers drew our attention to two recent publications from the Cole-Hamilton group concerning the photophysics of *para*-substituted biphenylvinyl OS compounds.[89,90] In one paper, an octa-3,5-dicarbaldehyde-biphenylvinyl OS compound, on reduction with NaBH$_4$, exhibited an estimated red-shift of 60 nm with respect to the NaBH$_4$-reduced dicarbaldehyde model compound, providing additional support for the arguments presented here.[89] In the second paper, on *para*-substituted biphenylvinyl OS compounds,[90] theoretical studies suggested the potential for intramolecular excited-state interactions. However, their formation was ruled out by the absence of structureless emission bands and the difficulty in forming such structures at room temperature in solution, especially with the bulky *para* substituents used. The latter study observed small red-shifts and much higher quantum yields for N-substituted derivatives than seen here, perhaps because the bulky *para* subsitutents interfere with the formation of charge-transfer states, as acknowledged by the authors. These authors also suggest that the observed red-shifts may arise for the reasons cited above.

During revision of this manuscript, a paper by Kieffer et al. was published describing the use of Frontier orbital analysis to characterize a set of aromatic-substituted SQs. That group found that these types of cages are at least partially conjugated and serve as electron acceptors, in agreement with our findings.[91]

Finally, the clean synthesis of all *ortho*-4-methylstilbene$_8$OS gives results that, although unexpected, support our contentions. The UV−vis spectrum (THF) shows a single λ_{max} at $\sim$300 nm with emission maxima at 402 and 426 nm, whereas an authentic sample of *trans*-4-methylstilbene (Table 4) exhibits UV−vis absorption maxima at 302 and 312 nm and an emission maximum λ_{max} at $\sim$352 nm. In addition, the methyl group in the NMR appears at 2.08 ppm, whereas that for *trans*-4-methylstilbene appears at 2.36 ppm. We originally thought that this indicated formation of *cis*-stilbene but find that the vinyl proton coupling constants are 16 Hz, indicative of a *trans* configuration. These differences suggest significant interactions of the 4-Mestilbene moieties with the cage face including the oxygens where the HOMO resides. The fact that the emission spectrum is red-shifted 50−60 nm and looks very similar to that for the *para*-4-methylstilbene$_8$OS suggests that the emissions are not from the π^* orbital localized solely on the stilbene moiety but rather from some 3-D excited state.

The implications of these findings are that these octafunctional molecules exhibit some form of 3-D interaction in the excited state that might permit their use as single-molecule transistors or organic light-emitting diodes as well as for energy collection and dispersion as molecular antennas, for example, and for NLO applications.[92−96]

Supporting Information Available: Detailed spectroscopic characterizations of the various compounds prepared in this work. This material is available free of charge via the Internet at http://pubs.acs.org.

JA9087709

(89) Vautravers, N. R.; Andre, P.; Cole-Hamilton, D. J. *J. Mater. Chem.* **2009**, *19*, 4545.
(90) Andre, P.; Cheng, G.; Ruseckas, A.; van Mourik, T.; Früchtl, H.; Crayston, J. A.; Morris, R. E.; Cole-Hamilton, D.; Samuel, I. D. W. *J. Phys. Chem. B* **2008**, *112*, 16382.
(91) Zhen, C.-G.; Becker, U.; Kieffer, J. *J. Phys. Chem. A* **2009**, *113*, 9707.

(92) Halim, M.; Pillow, J. N. G.; Samuel, I. D. W.; Burn, P. L. *Adv. Mater.* **1999**, *11*, 371.
(93) Wang, S.; Oldham, W. J., Jr.; Hudack, R. A., Jr.; Bazan, G. C. *J. Am. Chem. Soc.* **2000**, *122*, 5695.
(94) Freeman, A. W.; Koene, S. C.; Malenfant, P. R. L.; Thompson, M. E.; Frechet, J. M. J. *J. Am. Chem. Soc.* **2000**, *122*, 12385.
(95) Satoh, N.; Cho, J.-S.; Higuchi, M.; Yamamoto, K. *J. Am. Chem. Soc.* **2003**, *125*, 8104.
(96) Segura, J. L.; Gomez, R.; Martin, N.; Guldi, D. M. *Org. Lett.* **2001**, *3*, 2645.